



Ferromagnetism and exchange

Order, order, order!

Ferromagnetism and the Curie temperature were explained by Weiss in terms of a huge internal 'molecular field' proportional to the magnetization. The theory is applicable both to localized and delocalized electrons. No such magnetic field really exists, but it is a useful way of approximating the effect of the interatomic Coulomb interaction in quantum mechanics, which Heisenberg described by the Hamiltonian $\mathcal{H} = -2\mathcal{J}\mathbf{S}_1 \cdot \mathbf{S}_2$, where \mathbf{S}_1 and \mathbf{S}_2 are operators describing the localized spins on two adjacent atoms. When $\mathcal{J} > 0$, ferromagnetic exchange leads to ferromagnetic order in three dimensions. Spin waves are the low-energy excitations of the exchange-coupled magnetic lattice. In the delocalized electron picture, a ferromagnet has spontaneously spin-split energy bands. The density of \uparrow and \downarrow states is calculated using spin-dependent density functional theory. Important physical phenomena associated with ferromagnetism are discussed in this chapter, including magnetic anisotropy and, magnetoelastic, magneto-optic and magneto-transport effects.

The characteristic feature of a ferromagnet is its spontaneous magnetization M_s , which is due to alignment of the magnetic moments located on an atomic lattice. The magnetization tends to lie along easy directions determined by crystal structure, atomic-scale texture or sample shape. Heating above a critical temperature known as the Curie point, which ranges from less than 1 K for magnetically dilute salts to almost 1400 K for cobalt, leads to a reversible collapse of the spontaneous magnetization. Although there is no reason in principle why uniform ferromagnetic liquids should not exist, it seems that there are none. Ferrofluids, while ferromagnetic and liquid, are actually colloidal suspensions of solid ferromagnetic particles.

Important modifications of the electronic, thermal, elastic and optical properties are associated with magnetic order, whether ferromagnetic, or one of the more complex multisublattice or noncollinear ordered magnetic structures presented in the next chapter.

5.1 Mean field theory

5.1.1 Molecular field theory

The first modern theory of ferromagnetism, and one that remains useful today, was proposed by Pierre Weiss in 1906. Weiss's original theory was based on the classical paramagnetism of Langevin, but it was soon extended to the more general Brillouin theory of localized magnetic moments. His idea was that there is an internal 'molecular field' which is proportional to the magnetization of the ferromagnet. If n_W is the constant of proportionality, this adds to the internal contribution of any externally applied field:

$$\mathbf{H}^i = n_W \mathbf{M} + \mathbf{H}. \quad (5.1)$$

\mathbf{H}^i has to be enormous to induce a spontaneous magnetization at room temperature; the Weiss coefficient n_W is approximately 100. The magnetization is given by the Brillouin function (4.17) with $M_0 = nm_0 = ng\mu_B J$, where n is the number of magnetic atoms per unit volume,

$$M = M_0 \mathcal{B}_J(x), \quad (5.2)$$

but now

$$x = \mu_0 m_0 (n_W M + H) / k_B T. \quad (5.3)$$

In zero external field, \mathbf{M} is the spontaneous magnetization \mathbf{M}_s so we have

$$M_s / M_0 = \mathcal{B}_J(x_0), \quad (5.4)$$

where $x_0 = \mu_0 m_0 n_W M_s / k_B T$. Combining x_0 with $M_0 = nm_0$, we find $M_s / M_0 = (nk_B T / \mu_0 M_0^2 n_W) x_0$, which is conveniently written in terms of the Curie constant C (4.16) as

$$M_s / M_0 = [T(J + 1) / 3J C n_W] x_0. \quad (5.5)$$

The simultaneous solution of (5.4) and (5.5) is found graphically as indicated in Fig. 5.1. Otherwise the equations can be solved numerically. Results for M_s / M_0 versus T / T_C are plotted in Fig. 5.2 for some values of J , including the classical limit $J \rightarrow \infty$ where (5.4) is replaced by the Langevin function (4.21). In the Brillouin theory, the magnetization approaches zero temperature with horizontal slope, as required by thermodynamics (§2.5.4). Numerical values of the reduced spontaneous magnetization M_s / M_0 versus reduced temperature T / T_C are listed in Appendix G for different values of J . When S is the good quantum number, J in these formulae is replaced by S . Theory and experiment for nickel are compared in Fig. 5.3.

Weiss's molecular field theory was the first mean field theory of a phase transition. The moments are completely disordered at and above T_C , where the

Figure 5.1

Graphical solution of (5.4) and (5.5) for $J = \frac{1}{2}$ to find the spontaneous magnetization M_s when $T < T_c$. Equation (5.5) is also plotted for $T = T_c$ and $T > T_c$. The effect of an external field is to offset (5.5), as shown by the dotted line.

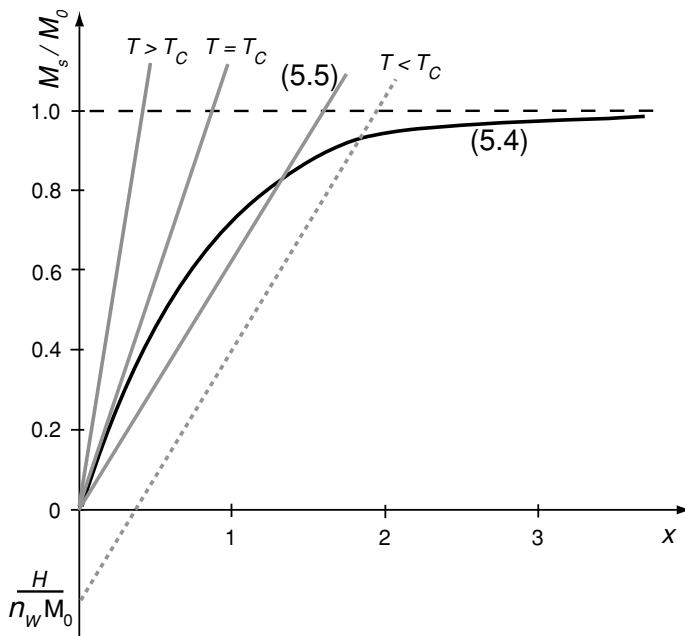
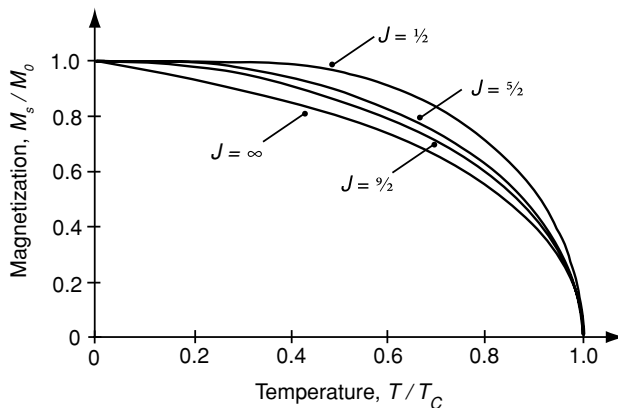


Figure 5.2

Spontaneous magnetization as a function of temperature calculated from molecular field theory, based on the Brillouin function for different values of J . The classical limit $J = \infty$ is based on the Langevin function.



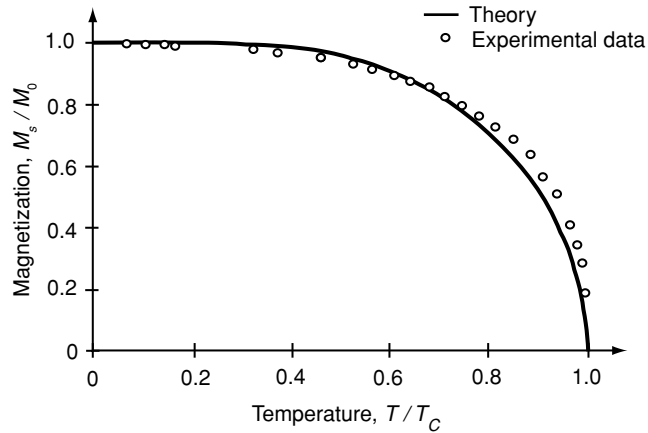
$2J + 1$ energetically degenerate M_J levels are equally populated. The magnetic entropy (4.25) then is $R \ln(2J + 1)$ per mole, where $R = N_A k_B$ is the gas constant, 8.315 J mol^{-1} . Below T_c , and especially just below, there is a specific heat of magnetic origin, as energy is absorbed to disorder the moments when the system is heated. A discontinuity in specific heat appears at T_c .

On a plot of M_s/M_0 versus x , the slope of (5.5) precisely at the Curie temperature is equal to the slope at the origin of the Brillouin function. For small x (4.19) $B_J(x) \approx [(J + 1)/3J]x$, hence there is a direct relation between Curie constant and Curie temperature:

$$T_c = n_w C. \tag{5.6}$$

Figure 5.3

The spontaneous magnetization for nickel, together with the theoretical curve for $J = \frac{1}{2}$ from the molecular field theory. Note that the theoretical curve is scaled to give correct values at each end.



In practice, T_C is used to determine n_W . Taking gadolinium as an example: $T_C = 292$ K, $J = S = 7/2$; $g = 2$; $n = 3.0 \times 10^{28} \text{ m}^{-3}$. Hence

$$C = \mu_0 n g^2 \mu_B^2 J(J+1)/3k_B \quad (4.16)$$

is 4.9 K, and the Weiss coefficient works out as $n_W = 59$.

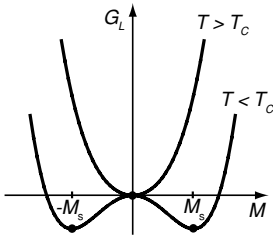
The paramagnetic susceptibility above T_C is obtained from (4.19), (5.3) and (5.4) in the small- x limit. The result is the Curie-Weiss law

$$\chi = C/(T - \theta_p), \quad (5.7)$$

where

$$\theta_p = T_C = \mu_0 n_W n g^2 \mu_B^2 J(J+1)/3k_B. \quad (5.8)$$

The Curie constant C is often written in terms of the effective moment m_{eff} as $C = \mu_0 n m_{\text{eff}}^2 / 3k_B$, where $m_{\text{eff}} = g\sqrt{J(J+1)}\mu_B$. In this theory, the paramagnetic Curie temperature θ_p is equal to the Curie temperature T_C , which is the point where the susceptibility diverges.



The Landau free energy for a ferromagnet at temperatures close to the Curie temperature. There are two energy minima at $\pm M_s$ for $T < T_C$, but a single minimum at $M = 0$ for $T > T_C$.

5.1.2 Landau theory

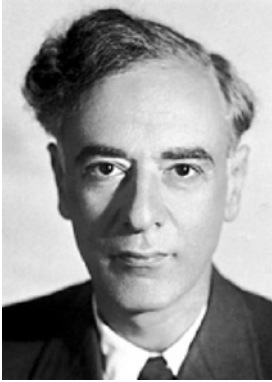
An approach that is equivalent to molecular field theory close to T_C , where M is small and aligned with any field external H' , is to expand the free energy G_L in even powers of M . Only even powers are permitted in the series, because time reversal symmetry requires that the energy is unchanged on reversing the magnetization, $G_L(M) = G_L(-M)$ in the absence of the external field:

$$G_L = AM^2 + BM^4 + \dots - \mu_0 H' M. \quad (5.9)$$

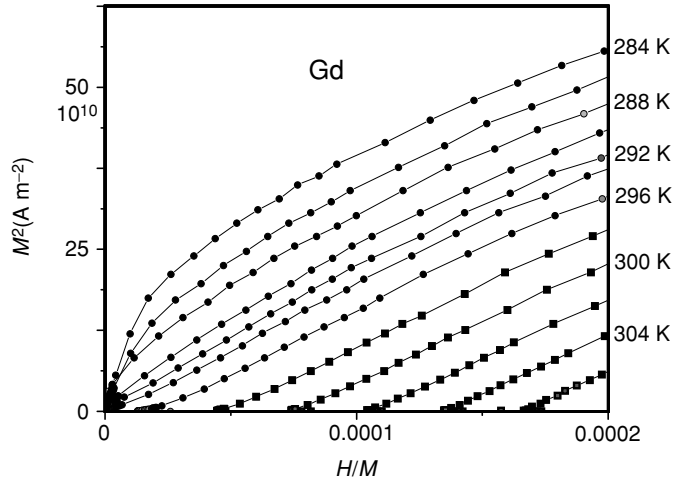
The coefficients A and B depend on temperature. There is a difference between the Landau free energy $G_L = f(M, T) - \mu_0 H' M$ and the Gibbs free energy $G(H', T) = F(M, T) - \mu_0 H' M$ (§2.5.4), where M is expressed as a function

Figure 5.4

Arrott-Belov plots to determine T_C for gadolinium. The experimentally measured magnetization is $\sigma = M d$, where d is the density, rather than M . (Data courtesy of M. Venkatesan.)



Lev Landau 1908-1968.



of the variables H' , T via the equation of state $M = M(H', T)$; G_L is the energy of the state when M is forced to adopt a particular value, as if it were an external constraint. G_L is minimized in a local energy minimum with that value of M , which makes the approach useful for treating problems of hysteresis.

For $T < T_C$, energy minima at $M = \pm M_s$ imply $A < 0$ and $B > 0$. For $T > T_C$ an energy minimum at $M = 0$ implies $A > 0$ and $B > 0$. It follows that A must change sign at T_C . It has the form $a(T - T_C)$, where a is a constant independent of temperature, $a > 0$. The equilibrium magnetization minimizes G_L with respect to M ; $\partial G_L / \partial M = 0$ implies

$$2AM + 4BM^3 = \mu_0 H'. \quad (5.10)$$

Close to T_C , in zero field, $M_s^2 = -A/2B$, hence

$$M_s \approx \sqrt{a/2B}(T_C - T)^{\frac{1}{2}}, \quad (5.11)$$

as shown in Fig. 5.2. Ignoring the demagnetizing field, the Curie-Weiss susceptibility M/H' is given by (5.10) as $\mu_0/2A$;

$$\chi \approx (\mu_0/2a)(T - T_C)^{-1}. \quad (5.12)$$

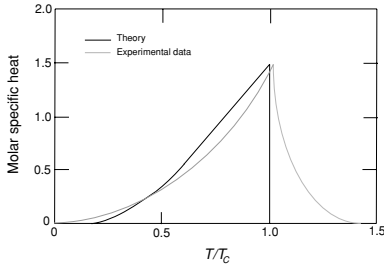
When the system is at a temperature exactly equal to T_C , $A = 0$ and (5.10) gives the critical isotherm

$$M = (\mu_0/4B)^{1/3} H'^{1/3}, \quad (5.13)$$

whereas in the vicinity of T_C (5.10) gives

$$M^2 = (\mu_0/4B)H'/M - (a/2B)(T - T_C). \quad (5.14)$$

This last equation is the basis of Arrott-Belov plots used for precise determination of the Curie temperature. The $M(H)$ curves at different temperatures are plotted



Comparison of the measured magnetic specific heat of a ferromagnet near T_C (dotted line) with the prediction of mean field theory (solid line).

as M^2 versus H'/M , and the isotherm that extrapolates to zero is the one at T_C (Fig. 5.4).

The magnetic specific heat C_m can also be calculated from Landau theory using $C_m = -T(\partial^2 G_L/\partial T^2)$. Results from (5.9) and (5.14) are $C_m = Ta^2/2B$ when $T = T_C^-$ and $C_m = 0$ when $T = T_C^+$. There is a stepwise discontinuity at T_C , with no magnetic specific heat above the transition where $M = 0$.

The Landau theory can be adapted to any continuous or discontinuous phase transition. M is the order parameter for the ferromagnet, H' is the conjugate field and the relation between them is the generalized susceptibility χ . Whatever the interpretation of these parameters in different physical systems, the power laws describing their variations with T near T_C are exactly the same. The same powers are obtained from Landau theory and from Weiss's molecular field theory. This can be verified by expanding the Brillouin function to order x^3 (4.19), which gives an expression equivalent to (5.9). Both are mean field theories of ferromagnetism. Other terms may be added to the free energy to include additional fields such as pressure or stress. It is remarkable how many relations can be established between different measurable physical quantities from an expansion of the free energy in powers of the order parameter.

The power law variations of the physical properties in the vicinity of T_C are summarized in Table 5.1. The values of the static critical exponents $\alpha, \beta, \gamma, \delta$ are common to all mean field theories.

Experimentally, the properties of ferromagnets do show power law behaviour in $(T - T_C)$ provided measurements are made sufficiently close to the Curie point, but the critical exponents are somewhat different from those predicted by mean field theory. For example, ferromagnets usually show a λ -type anomaly in their specific heat at T_C , rather than a stepwise discontinuity. The divergence is described by a critical exponent $\alpha \approx 0.1$, rather than zero. The residual magnetic specific heat above T_C is witness to the persistence of short-range order, which is not predicted by the theory. Above T_C , the susceptibility follows a power law $\chi \sim (T - T_C)^{-\gamma}$, where γ is about 1.3, whereas in mean field theory γ is 1 (the Curie–Weiss law). The critical exponents $\alpha, \beta, \gamma, \delta$ for nickel, for example, are 0.10, 0.42, 1.32 and 4.5, respectively. We return to this topic at the end of Chapter 6.

The other place where significant deviations from the mean field theory are found is at low temperatures, where the spin-wave excitations discussed later in the chapter are important.

Table 5.1. The critical exponents of a mean field ferromagnet

Specific heat	$C_m \sim T_C - T ^\alpha$	$\alpha = 0$
Magnetization	$M_s \sim (T_C - T)^\beta$	$\beta = \frac{1}{2}$
Susceptibility	$\chi \sim (T - T_C)^{-\gamma}$	$\gamma = 1$
Critical isotherm	$M_s \sim H^{1/\delta}$	$\delta = 3$

Table 5.2. Dimensionless susceptibility of some metals at 298 K (units: 10^{-6})

Li	14	Sc	263	Cu	-10	Ce	1778
K	6	Y	121	Zn	-16	Nd	3433
Be	-24	Ti	182	Au	-34	Eu	15570
Ca	22	Nb	237	Al	21	Gd	476300
Ba	7	Mo	123	Sn	-29	Dy	68400
		Pd	805	Bi	-164	Tm	17710
		Pt	279				

5.1.3 Stoner criterion

The starting point for a discussion of ferromagnetism in metals is the band paramagnetism introduced in §3.2.6. The Pauli susceptibility is a small, positive quantity, practically independent of temperature because delocalized electrons obey Fermi–Dirac statistics; only the small fraction of them with energy close to ε_F are able to respond to a change in temperature or magnetic field.

In the three-dimensional free-electron model, the density of states $\mathcal{D}(\varepsilon)$ (states $\text{m}^{-3} \text{J}^{-1}$) varies as $\sqrt{\varepsilon}$ (3.39), and the \uparrow and \downarrow bands shift by $\mp \mu_0 H \mu_B$ in the field as shown in Fig. 3.7. The resulting susceptibility (3.43) can be written

$$\chi_P = \mu_0 \mu_B^2 \mathcal{D}(\varepsilon_F), \quad (5.15)$$

where $\mathcal{D}(\varepsilon_F)$ is the density of states at the Fermi level for both spins, which is double the density of states for one spin $\mathcal{D}_{\uparrow, \downarrow}(\varepsilon_F)$. The Pauli susceptibility is approximately 10^{-5} for many metals, but it approaches 10^{-3} for the $4d$ metal Pd (Table 5.2). Narrower bands tend to have higher susceptibility, because the density of states at ε_F scales as the inverse of the bandwidth. When the density of states is high enough, it becomes energetically favourable for the bands to split, and the metal becomes spontaneously ferromagnetic.

Stoner applied Weiss's molecular field idea to the free-electron gas. Assuming the linear variation of internal field with magnetization has a coefficient n_S :

$$H^i = n_S M + H, \quad (5.16)$$

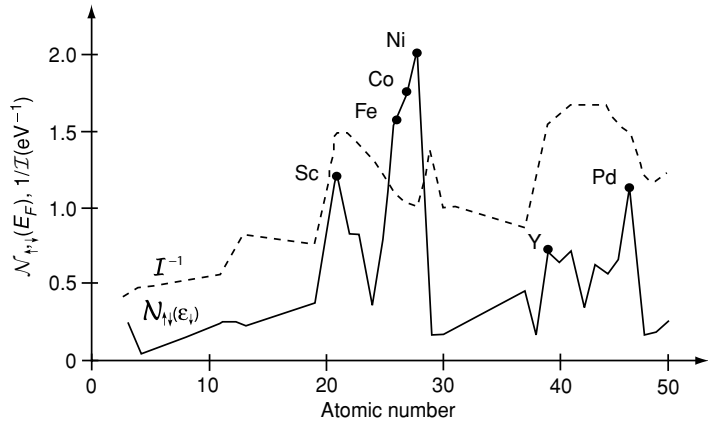
the Pauli susceptibility in the internal field is $\chi_P = M/(n_S M + H)$. Hence, the response to the field H

$$\chi = M/H = \chi_P/(1 - n_S \chi_P) \quad (5.17)$$

is a susceptibility that is enhanced when $n_S \chi_P < 1$ and diverges when $n_S \chi_P = 1$. Stoner expressed this condition in terms of the local density of states at the Fermi level, $\mathcal{D}(\varepsilon_F)$. Writing the exchange energy (in J m^{-3}) $-\frac{1}{2} \mu_0 H^i M = -\frac{1}{2} \mu_0 n_S M^2$ as $-(\mathcal{I}/4)(n^\uparrow - n^\downarrow)^2/n$, where $M = (n^\uparrow - n^\downarrow)\mu_B$

Figure 5.5

Comparison of $\mathcal{N}_{\uparrow,\downarrow}(\varepsilon_F)$ with $1/\mathcal{I}$ for metallic elements.



and n is the number of atoms per unit volume, it follows from (5.15) that $n_S \chi_P = \mathcal{I} \mathcal{D}(\varepsilon_F) / 2n$. The metal becomes spontaneously ferromagnetic when the susceptibility diverges spontaneously; in other words when

$$\mathcal{I} \mathcal{N}_{\uparrow,\downarrow}(\varepsilon_F) > 1, \quad (5.18)$$

where $\mathcal{N}_{\uparrow,\downarrow}(\varepsilon) = \mathcal{D}(\varepsilon) / 2n$ is the density of states per atom for each spin state. This is the famous Stoner criterion. The Stoner exchange parameter \mathcal{I} is roughly 1 eV for the 3d ferromagnets, and $n_S \gtrsim 10^3$ for spontaneous band splitting. The exchange parameter has to be comparable to the width of the band for spontaneous splitting to be observed. Ferromagnetic metals have narrow bands and a peak in the density of states $\mathcal{N}(\varepsilon)$ at or near ε_F . The data in Fig. 5.5 show that only Fe, Co and Ni meet the Stoner criterion. Pd comes close.

5.2 Exchange interactions

The origin of the effective field \mathbf{H}^i is the exchange interaction, which reflects the Coulomb repulsion of two nearby electrons, usually on neighbouring atoms, acting in conjunction with the Pauli principle, which forbids the two electrons to enter the same quantum state. Electrons cannot be in the same place if they have the same spin. There is an energy difference between the $\uparrow_i \uparrow_j$ and $\uparrow_i \downarrow_j$ configurations of the spins of neighbouring atoms i, j . Interatomic exchange in insulators is usually one or two orders of magnitude weaker than the ferromagnetic intra-atomic exchange between electrons on the same atom, which leads to Hund's first rule.

As stated in §4.1, the Pauli principle forbids more than one electron to enter a quantum state, denoted by a particular set of quantum numbers. Electrons are indistinguishable, so exchange of two electrons must give the same electron density $|\Psi(1, 2)|^2 = |\Psi(2, 1)|^2$. Since electrons are fermions, the only solution

is for the total wave function of the two electrons to be antisymmetric

$$\Psi(1, 2) = -\Psi(2, 1). \quad (5.19)$$

The total wave function Ψ is the product of functions of space and spin coordinates $\phi(\mathbf{r}_1, \mathbf{r}_2)$ and $\chi(s_1, s_2)$.

The simple example of the hydrogen molecule H_2 with two atoms each having an electron in a hydrogenic $1s$ -orbital $\psi_i(\mathbf{r}_i)$ gives an idea of the physics of exchange. Schrödinger's equation is $\mathcal{H}(\mathbf{r}_1, \mathbf{r}_2)\Psi(\mathbf{r}_1, \mathbf{r}_2) = \varepsilon\Psi(\mathbf{r}_1, \mathbf{r}_2)$ where, neglecting the interactions between the electrons,

$$\left[-\frac{\hbar^2}{2m} \left(\frac{\partial^2}{\partial r_1^2} + \frac{\partial^2}{\partial r_2^2} \right) - \frac{e^2}{4\pi\epsilon_0} \left(\frac{1}{r_1} + \frac{1}{r_2} \right) \right] \Psi(\mathbf{r}_1, \mathbf{r}_2) = \varepsilon\Psi(\mathbf{r}_1, \mathbf{r}_2). \quad (5.20)$$

There are two molecular orbits, a spatially symmetric bonding orbital ϕ_s , with electronic charge piled up between the atoms, and a spatially antisymmetric antibonding orbital ϕ_a having a nodal plane with no charge midway between them. Chemical bonds which involve hybridized wave functions of electrons of neighbouring atoms are generally classified in this way:

$$\phi_s = (1/\sqrt{2})(\psi_1 + \psi_2) \quad \phi_a = (1/\sqrt{2})(\psi_1 - \psi_2). \quad (5.21)$$

ψ_1 and ψ_2 are the spatial components of the individual wave functions of electrons 1 and 2 respectively. The wave functions $\psi_1(\mathbf{r}_1)$ and $\psi_2(\mathbf{r}_2)$ are the solutions of Schrödinger's equation for each individual atom.

The symmetric and antisymmetric spin functions are the spin triplet and spin singlet states:

$$S = 1; \quad M_S = 1, 0, -1$$

$$\chi_s = |\uparrow_1, \uparrow_2\rangle; \quad (1/\sqrt{2})[|\uparrow_1, \downarrow_2\rangle + |\downarrow_1, \uparrow_2\rangle]; \quad |\downarrow_1, \downarrow_2\rangle$$

$$S = 0; \quad M_S = 0$$

$$\chi_a = (1/\sqrt{2})[|\uparrow_1, \downarrow_2\rangle - |\downarrow_1, \uparrow_2\rangle]$$

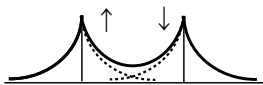
According to (5.19), the symmetric space function must multiply the antisymmetric spin function, and vice versa. Hence the total antisymmetric wave functions are

$$\Psi_I = \phi_s(1, 2)\chi_a(1, 2),$$

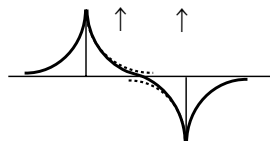
$$\Psi_{II} = \phi_a(1, 2)\chi_s(1, 2).$$

When the two electrons are in a spin triplet state, there can be no chance of finding them at the same point of space. Electrons with parallel spins avoid each other. But if the electrons are in the spin singlet state, with antiparallel spins, there is some probability of finding them in the same place, because the spatial part of the wave function is symmetric under exchange of the electrons.

$S = 0$



$S = 1$



The spatially symmetric and antisymmetric wave functions for the H_2 molecule.

The energies of the two states can be evaluated from the Hamiltonian $\mathcal{H}(\mathbf{r}_1, \mathbf{r}_2)$ in (5.20):

$$\varepsilon_{I,II} = \int \phi_{s,a}^*(\mathbf{r}_1, \mathbf{r}_2) \mathcal{H}(\mathbf{r}_1, \mathbf{r}_2) \phi_{s,a}(\mathbf{r}_1, \mathbf{r}_2) d\mathbf{r}_1^3 d\mathbf{r}_2^3.$$

For the hydrogen molecule, ε_I is lower than ε_{II} . In other words, the bonding orbital/spin singlet state lies below the antibonding orbital/spin triplet state because of the spatial constraint on the triplet. Setting the exchange integral $\mathcal{J} = (\varepsilon_I - \varepsilon_{II})/2$, we can write the energy in the form

$$\varepsilon = -2(\mathcal{J}/\hbar^2) \mathbf{s}_1 \cdot \mathbf{s}_2, \quad (5.22)$$

where the product $\mathbf{s}_1 \cdot \mathbf{s}_2$ is $\frac{1}{2}[(s_1 + s_2)^2 - s_1^2 - s_2^2]$. According to whether the spin quantum number $S = s_1 + s_2$ is 0 or 1, the eigenvalues are $-\frac{3}{4}\hbar^2$ or $+\frac{1}{4}\hbar^2$. The energy splitting between the singlet state Ψ_I and the triplet state Ψ_{II} is $2\mathcal{J}$. Here \mathcal{J} is the exchange integral

$$\mathcal{J} = \int \psi_1^*(\mathbf{r}') \psi_2^*(\mathbf{r}) \mathcal{H}(\mathbf{r}, \mathbf{r}') \psi_1(\mathbf{r}) \psi_2(\mathbf{r}') d\mathbf{r}^3 d\mathbf{r}'^3.$$

In the H_2 molecule, the spin singlet state is lower, so the integral is negative. In an atom, however, the orbitals are orthogonal and \mathcal{J} is positive.

Heisenberg generalized (5.22) to many-electron atomic spins \mathbf{S}_1 and \mathbf{S}_2 , writing his famous Hamiltonian

$$\mathcal{H} = -2\mathcal{J} \hat{\mathbf{S}}_1 \cdot \hat{\mathbf{S}}_2, \quad (5.23)$$

where $\hat{\mathbf{S}}_1$ and $\hat{\mathbf{S}}_2$ are dimensionless spin operators, like the Pauli spin matrices in (3.17). The \hbar^2 has been absorbed into the exchange constant \mathcal{J} , which has units of energy. From now on we will adopt this convention, in order to avoid writing \hbar everywhere. We also drop the hat on the spin operators, $\hat{\mathbf{S}}_i$. The exchange integral \mathcal{J} then has dimensions of energy, and it is often expressed in kelvins by dividing it by k_B , Boltzmann's constant. $\mathcal{J} > 0$ indicates a ferromagnetic interaction, which tends to align the two spins parallel; $\mathcal{J} < 0$ indicates an antiferromagnetic interaction, which tends to align the two spins antiparallel.

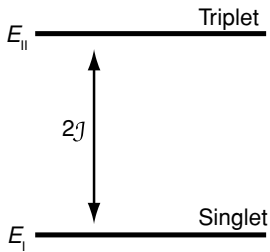
When there is a lattice, the Hamiltonian¹ is generalized to a sum over all pairs of atoms on lattice sites i, j :

$$\mathcal{H} = -2 \sum_{i>j} \mathcal{J}_{ij} \mathbf{S}_i \cdot \mathbf{S}_j. \quad (5.24)$$

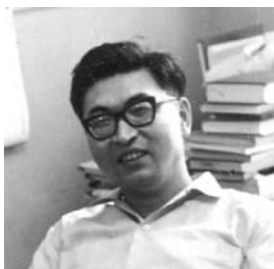
This is simplified to a sum with a single exchange constant \mathcal{J} if only nearest-neighbour interactions count. The interatomic exchange coupling described by the Heisenberg Hamiltonian can only be ferromagnetic or antiferromagnetic.

The Heisenberg exchange constant \mathcal{J} can be related to the Weiss constant n_W of the molecular field theory. Suppose that a moment $g\mu_B S_i$ interacts with an effective field $H^i = n_W M = n_W n g \mu_B S$, and that in the Heisenberg model

¹ Other conventions exist, omitting the 2 and/or counting each pair in the sum twice.



Splitting of the spin singlet and spin triplet states for the H_2 molecule. The exchange integral \mathcal{J} is negative, so the singlet is lower.



Junjiro Kanamori, 1930-.

only the nearest neighbours of S_i interact appreciably with it. Then the site Hamiltonian is

$$\mathcal{H}_i = -2 \left[\sum_j \mathcal{J} S_j \right] \cdot S_i \approx -\mu_0 H^i g \mu_B S_i. \quad (5.25)$$

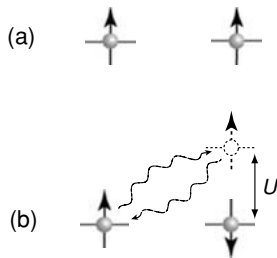
The molecular field approximation amounts to averaging out the local correlations between S_i and S_j . If Z is the number of nearest neighbours in the sum, then $\mathcal{J} = \mu_0 n_W n g^2 \mu_B^2 / 2Z$. Hence, from (5.8)

$$T_C = \frac{2Z\mathcal{J}S(S+1)}{3k_B}. \quad (5.26)$$

Taking the example of gadolinium again, where $T_C = 292$ K, $S = 7/2$, $Z = 12$, we find $\mathcal{J}/k_B = 2.3$ K.

The Heisenberg Hamiltonian (5.23) indicates that exchange interactions couple the atomic *spins*. It can be applied directly to the $3d$ elements, where the crystal field ensures that spin is a good quantum number, and to the rare-earth ions Eu^{2+} and Gd^{3+} , which have no orbital moment. However, J is the good quantum number for the other rare-earths, so S must be projected onto J , as explained below. Ions with a $J = 0$ ground-state multiplet, Sm^{2+} and Eu^{3+} , cannot order magnetically despite their large spin quantum number, $S = 3$.

Generally, the energy of any electronic system is lowered as the wave functions spread out. This follows from the uncertainty principle $\Delta p \Delta x \approx \hbar$. When many more-or-less delocalized electrons are present in different orbitals, the calculation of exchange is a delicate matter. Orbital degeneracy, absent in the H_2 molecule, opens the possibility that triplet states may be lower in energy than singlets. The energies involved are only ≈ 1 meV, compared with bandwidths of order 1–10 eV. Competing exchange interactions may coexist with different signs of coupling. It is therefore best to describe exchange phenomenologically, and determine the exchange interactions experimentally.



The antiferromagnetic superexchange interaction. Two neighbouring sites with singly occupied orbitals are shown with (a) parallel or (b) antiparallel spin alignment. Hopping is forbidden by the Pauli principle in the parallel case. There is an energy gain due to virtual hopping in the antiparallel case.

5.2.1 Exchange in insulators

Superexchange The electrons in insulators are localized. Oxides are a good example. There is little direct $3d$ – $3d$ overlap in transition-metal oxides, but the $3d$ -orbitals are hybridized with the oxygen $2p$ -orbitals; $\phi_{3d} = \alpha\psi_{3d} + \beta\psi_{2p}$ with $|\alpha|^2 + |\beta|^2 = 1$. The oxygen bridges transmit a ‘superexchange’ interaction, which can be described by the Heisenberg Hamiltonian.

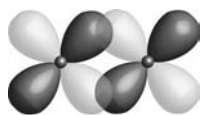
Figure 5.6 shows a typical superexchange bond. In the case of a singly occupied $3d$ -orbital or a half-filled d shell (Fe^{3+} , Mn^{2+}), configuration (b) is lower in energy than configuration (a) because both electrons in an oxygen $2p$ -orbital can then spread out into unoccupied $3d$ -orbitals. The superexchange interaction \mathcal{J} involves simultaneous virtual transfer of two electrons with the instantaneous formation of a $3d^{n+1}2p^5$ excited state; the interaction is of order $-2t^2/U$, where t is the p – d transfer integral and U is the on-site $3d$ Coulomb

Figure 5.6

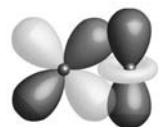
A typical superexchange bond. Configuration (b) is lower in energy than configuration (a).



John B. Goodenough, 1922-.

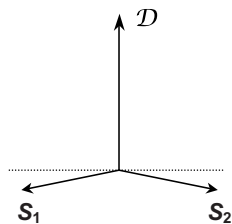


(a)

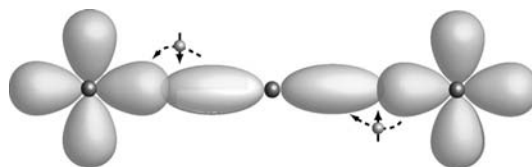


(b)

Overlapping d -orbitals characterized by (a) nonzero and (b) zero overlap integrals. Dark and light shading denotes positive and negative sign of the wave function.



Canted antiferromagnetism due to the Dzyaloshinski-Moriya interaction.



3d(Mn) 2p(O) 3d(Mn)



interaction. The transfer integral is of order 0.1 eV and the on-site Coulomb interaction is in the range 3–5 eV. \mathcal{J} depends sensitively on the interatomic separation, but also on the M–O–M bond angle, varying as $\cos^2 \theta_{12}$.

The occupancy and orbital degeneracy of the 3d states is the critical factor in determining the strength and sign of superexchange. There are many possible cases to consider and the results were summarized in the Goodenough–Kanamori rules. The rules were reformulated by Anderson, in a simpler way that makes it unnecessary to consider the oxygen.

- (i) When two cations have lobes of singly occupied 3d-orbitals which point towards each other giving large overlap and hopping integrals, the exchange is strong and *antiferromagnetic* ($\mathcal{J} < 0$). This is the usual case, for 120–180° M–O–M bonds.
- (ii) When two cations have an overlap integral between singly occupied 3d-orbitals which is zero by symmetry, the exchange is *ferromagnetic* and relatively weak. This is the case for $\sim 90^\circ$ M–O–M bonds.
- (iii) When two cations have an overlap between singly occupied 3d orbitals and empty or doubly occupied orbitals of the same type, the exchange is also *ferromagnetic*, and relatively weak.

Superexchange is more commonly antiferromagnetic than ferromagnetic, because the overlap integrals are more likely to be large than zero.

Antisymmetric exchange A few materials with low symmetry exhibit a weak antisymmetric coupling, the Dzyaloshinski–Moriya interaction. This is represented by the Hamiltonian

$$\mathcal{H} = -\mathcal{D} \cdot (\mathcal{S}_i \times \mathcal{S}_j), \quad (5.27)$$

where \mathcal{D} is a vector which lies along a high-symmetry axis, so the tendency is to couple the two spins *perpendicularly*. This is a higher-order effect, occurring between ions already coupled by superexchange; $|\mathcal{D}/\mathcal{J}| \approx 10^{-2}$. In an antiferromagnet, the spins may be canted away from the antiferromagnetic axis by about 1° . Antisymmetric exchange is the reason why antiferromagnets with a uniaxial crystal structure such as MnF_2 , MnCO_3 and $\alpha\text{Fe}_2\text{O}_3$ may exhibit a weak ferromagnetic moment. In the older literature the term parasitic

ferromagnetism is encountered for this kind of intrinsic weak ferromagnetism, because it was thought to be due to ferromagnetic impurities. A moment only appears when the antiferromagnetic axis is perpendicular to the crystallographic axis of symmetry, along which \mathcal{D} is constrained to lie. It disappears when the axes are parallel.

Biquadratic exchange This is another weak, higher-order effect which is sometimes detectable for the rare-earths. It is represented by the Hamiltonian

$$\mathcal{H} = -\mathcal{B}(\mathbf{S}_i \cdot \mathbf{S}_j)^2. \quad (5.28)$$

5.2.2 Exchange in metals

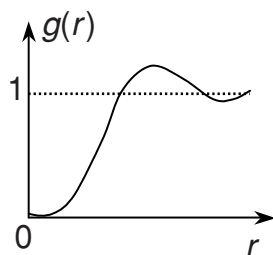
The principal exchange mechanism in ferromagnetic and antiferromagnetic metals involves overlap of the partly localized atomic orbitals of adjacent atoms. Other exchange mechanisms involve the interaction of purely delocalized electrons or of localized and delocalized electrons in the metal.

Direct exchange In $3d$ metals, the electrons are described by extended wave functions and a spin-polarized local density of states. It is usually more appropriate to describe them by the one-electron d wave functions of §4.4.2, rather than the free-electron waves of §3.2.5. In the tight-binding model the overlap of the one-electron wave functions is small and the electrons remain mostly localized on the atoms. The model Hamiltonian is

$$\mathcal{H} = \sum_{ij} t_{ij} c_i^\dagger c_j,$$

where the sum represents the conduction band in terms of the electron creation and annihilation operators² c^\dagger and c . Usually only nearest-neighbour interactions are important and the interatomic transfer integral $t_{ij} = t$. The bandwidth in the tight-binding model is $W = 2Zt$, where Z is the number of nearest neighbours. In $3d$ metals $t \approx 0.1$ eV and $Z = 8 - 12$, so the d bands are a few eV wide. Exchange in a roughly half-filled band is antiferromagnetic, because the energy gain associated with letting the wave functions expand onto neighbouring sites is only achieved when the neighbours are antiparallel, leaving empty \uparrow orbitals on the neighbouring sites to transfer into. Nearly filled or nearly empty bands tend to be ferromagnetic (Fig. 5.7) because electrons can then hop into empty states with the same spin. This helps to explain why chromium and manganese are antiferromagnetic, but iron, cobalt and nickel are ferromagnetic.

Bandwidth is the enemy of exchange. As t becomes large, the electrons are delocalized regardless of their spin. The alkali metals, for example, are Pauli

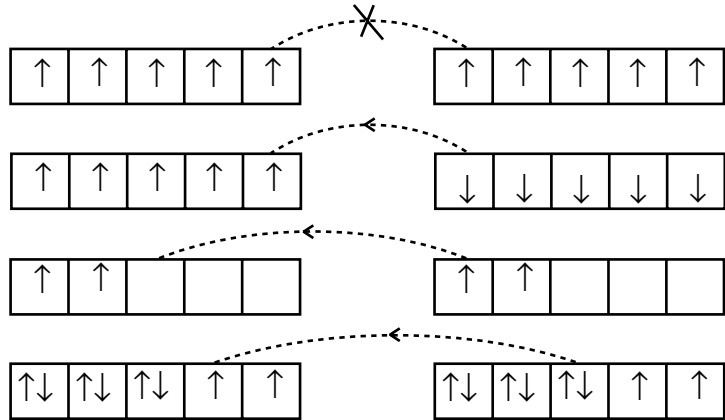


The exchange hole: the normalized probability of finding two electrons with the same spin a distance r apart.

² c_j is an operator that destroys an electron on site j , while c_i^\dagger is an operator that creates an electron on site i . The product $c_i^\dagger c_j$ therefore transfers an electron from site j to site i .

Figure 5.7

Electron delocalization in d bands which are half-full, almost empty or almost full.



paramagnets described by a free-electron model with one electron per atom. The early $3d$ metals scandium, titanium and vanadium are not ferromagnetic because t is too big. Scandium comes close. If it were possible to dilate the lattice to reduce t a little, scandium would become ferromagnetic.

The sign of the direct exchange depends principally on band occupancy, and then on the interatomic spacing, with ferromagnetic exchange favoured at larger spacing. The exchange is greatest just after the critical condition for the appearance of magnetism, $U/W > (U/W)_{crit}$, where U is the on-site Coulomb interaction, and W is the bandwidth.

s - d model Coupling of the spins s of the conduction electrons with core spins S in a metal is generally represented by a Hamiltonian including the term

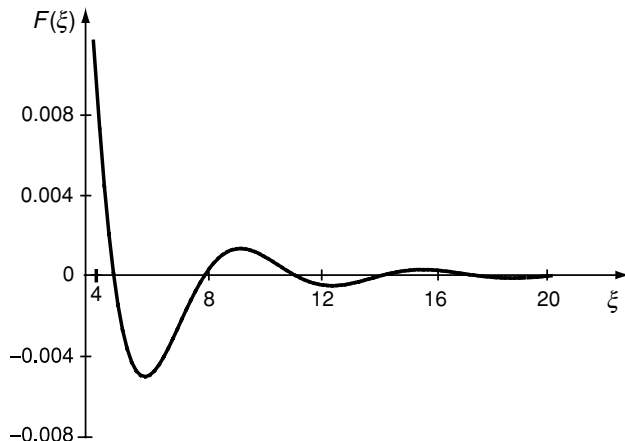
$$-\mathcal{J}_{sd}\Omega|\psi|^2\mathbf{S}\cdot\mathbf{s}, \quad (5.29)$$

where Ω is the volume of the core d shell and $|\psi|^2$ is the s -electron probability density. The s - d coupling is an on-site interaction, so the coupling constant is large, $\mathcal{J}_{sd} \approx 1$ eV. This interaction may lead to long-range ferromagnetic coupling between the core spins, regardless of whether \mathcal{J}_{sd} is positive or negative. The host conduction band is supposed to be uniformly spin-polarized parallel or antiparallel to the core spins.

RKKY interaction The ' s - d ' model applies as well to rare-earths, where the core spins are not $3d$, but $4f$. The localized moments in the $4f$ shell interact via electrons in the $5d/6s$ conduction band. The on-site interaction between a core spin S and a conduction electron spin s is $-\mathcal{J}_{sf}\mathbf{S}\cdot\mathbf{s}$, where $\mathcal{J}_{sf} \approx 0.2$ eV. Ruderman, Kittel, Kasuya and Yosida showed that a single magnetic impurity actually creates a nonuniform, oscillating spin polarization in the conduction band which falls off as r^{-3} . This spin polarization is related to the Friedel oscillations of charge density around the impurity which have wavelength π/k_F . It leads to long-range oscillatory coupling between core spins. For free

Figure 5.8

The RKKY function $F(\xi)$. Note that $F(\xi)$ becomes very large when $\xi < 4$.



electrons, the polarization is proportional to the RKKY function

$$F(\xi) = (\sin \xi - \xi \cos \xi)/\xi^4,$$

where $\xi = 2k_F r$, k_F being the Fermi wavevector (Fig. 5.8). This oscillating spin polarization results from the different potential seen by the \uparrow and \downarrow conduction electrons at the local moment site. The first zero of $F(\xi)$ is at $\xi = 4.5$. The effective coupling between two localized spins is

$$\mathcal{J}_{\text{eff}} \approx \frac{9\pi \mathcal{J}_{sf}^2 v^2 F(\xi)}{64 \mathcal{E}_F}, \quad (5.30)$$

where v is the number of conduction electrons per atom and \mathcal{E}_F is the Fermi energy. Since the Fermi wavevector is about 0.1 nm^{-1} (Table 3.3), the sign of \mathcal{J}_{eff} fluctuates on a scale of nanometres. When only ferromagnetic nearest-neighbour coupling is important, the Curie temperature can be deduced from (5.26). The RKKY interaction in the low-electron-density limit is equivalent to the s - d model with ferromagnetic coupling. Analogous oscillatory exchange is found in ferromagnetic multilayers with nonmagnetic spacer layers.

Among the rare-earth metals, only gadolinium has S as a good quantum number. The others have J as their quantum number, yet the exchange interaction couples spins. We therefore need to project S onto J when calculating the exchange coupling, whether direct or indirect. Since $\mathbf{L} + 2\mathbf{S} = g\mathbf{J}$ and $\mathbf{J} = \mathbf{L} + \mathbf{S}$, $\mathbf{S} = (g-1)\mathbf{J}$. This introduces a factor $(g-1)^2 J(J+1)$ into the exchange coupling. The factor is squared, because the spin enters the exchange interaction between two rare-earths twice. The effective coupling is

$$\mathcal{J}_{\text{RKKY}} = G \mathcal{J}_{\text{eff}}.$$

where $G = (g-1)^2 J(J+1)$ is the de Gennes factor. Magnetic ordering temperatures for any series of rare-earth metals or compounds with the same conduction-band structure and similar lattice spacings should scale with G ,

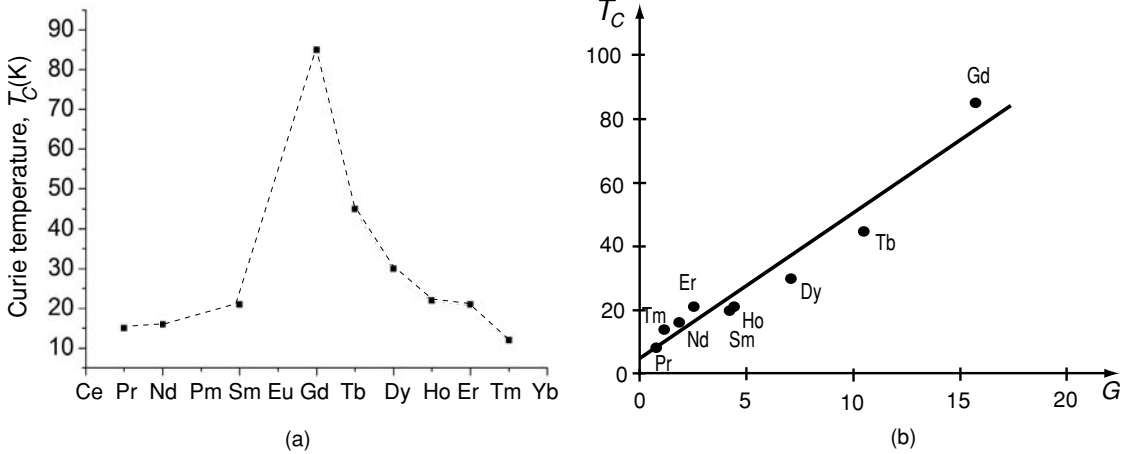


Figure 5.9

(a) Curie temperatures of ferromagnetic RNi_2 compounds; (b) a plot of T_C versus the de Gennes factor G .

and show a maximum for gadolinium. The de Gennes factor was included in Table 4.10. Figure 5.9 displays data for the Curie temperature of a series of ferromagnetic RNi_2 compounds. When plotted versus G , the data follow a straight line. The nickel in this series of intermetallic compounds is nonmagnetic.

Double exchange This interaction arises between $3d$ ions which have both localized and delocalized d electrons. Unlike ferromagnetic superexchange, mixed valence configurations are required for double exchange, as they are in any metal, but unlike a normal metal, the number of configurations is restricted to just two. In copper, for example, with its one electron in a broad $4s$ band, the instantaneous atomic configurations are s^0 , s^1 and s^2 . Electronic correlations are weak in broad bands, so the three configurations will appear with probabilities of $\frac{1}{4}$, $\frac{1}{2}$ and $\frac{1}{4}$. By contrast, a double-exchange material, such as the manganite $(\text{La}_{0.7}\text{Ca}_{0.3})\text{MnO}_3$, has both Mn^{4+} and Mn^{3+} ions (d^3 and d^4) present on octahedral sites. The two Mn valence states are imposed by the charge states of the other ions in the compound, La^{3+} , Ca^{2+} and O^{2-} . The d^3 core electrons for both octahedrally coordinated ions are localized in a narrow t_{2g}^{\uparrow} band, but the fourth d electron inhabits a broader e_g^{\uparrow} band, hybridized with oxygen, where it can hop from one d^3 core to another, Fig. 5.10. The configurations $d_i^3 d_j^4$ and $d_i^4 d_j^3$ on adjacent sites i and j are practically degenerate. On each site, there is strong on-site Hund's rule exchange coupling $\mathcal{J}_H \approx 2$ eV between t_{2g} and e_g electrons. Electrons can hop freely if the core spins are parallel, but when they are antiparallel there is a large energy barrier due to the Hund's rule interaction. If the quantization axes of adjacent sites are misaligned by an angle θ , the eigenvector of a \uparrow electron in the rotated frame is $\begin{pmatrix} \cos \theta/2 \\ \sin \theta/2 \end{pmatrix}$ (3.24). The transfer integral t therefore varies as $\cos(\theta/2)$. Double exchange is ferromagnetic because the transfer is zero when the ions on adjacent sites are antiparallel, $\theta = \pi$.

Figure 5.10

The double-exchange interaction. The electron hops with spin memory from one localized ion core to the next.

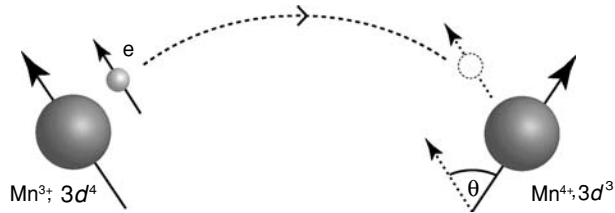
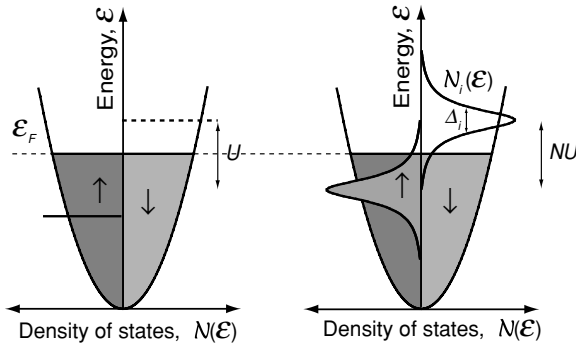


Figure 5.11

The Anderson impurity model. Local density of states for a magnetic impurity in a metal. On the left is shown the case where there is no mixing of the wave functions of the impurity level with the conduction electrons, on the right is the result of such hybridization.



Another common double-exchange pair is Fe^{3+} and Fe^{2+} , which are d^5 and d^6 ions respectively. The d^5 configuration is a half-filled \uparrow shell, and the sixth d electron occupies the bottom of a t_{2g}^{\downarrow} band when the ion is octahedrally coordinated by oxygen where it can hop directly from one d^5 core to another.

5.3 Band magnetism

5.3.1 Magnetic impurities in nonmagnetic metals

The above discussion of exchange between localized moments and conduction electrons in a metal begs the question of whether a magnetic impurity can really retain its moment when diluted in a nonmagnetic matrix. Does a single atom of cobalt, for example, still have a moment when it is diluted in copper? The magnetic impurity problem engrossed the magnetism community in the 1960s and 1970s. The $3d$ electrons of cobalt will hybridize with the $4s$ electrons of copper, broadening the local atomic level into a Lorentzian-like feature in the density of states. Figure 5.11 shows the energy level of a singly occupied d orbital before hybridization, with the doubly occupied orbital higher in energy by the on-site Coulomb repulsion energy U . Hybridization with the conduction band states broadens the impurity level, giving it a width Δ_i . Anderson showed that a moment, albeit one reduced by hybridization, is stable provided $U > \Delta_i$. Further broadening of the local density of states destroys the moment



P. W. Anderson 1923-.

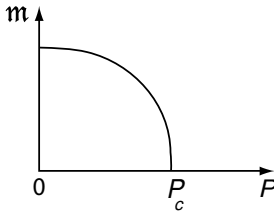
completely. The broadening is more effective for p -metals than for s -metals, because more electrons are available to hybridize with the impurity d -orbitals. Cobalt keeps its moment in copper, but loses it in aluminium.

The number of unpaired impurity electrons $N = N^\uparrow - N^\downarrow$ is

$$N = \nu(\varepsilon_F^+) - \nu(\varepsilon_F^-), \quad (5.31)$$

where $\varepsilon_F^\pm = \varepsilon_F \pm \frac{1}{2}NU$ and $\nu(\varepsilon)$, is the integral of the impurity density of states, $\int_0^\varepsilon \mathcal{N}_i(\varepsilon')d\varepsilon'$. Expanding this expression as a power series for small N , we find $N = NU\mathcal{N}_i(\varepsilon_F) + \frac{1}{24}(NU)^3\mathcal{N}_i''(\varepsilon_F)$, where the second derivative $\mathcal{N}_i''(\varepsilon) = d^2\mathcal{N}_i(\varepsilon)/d\varepsilon^2$ is negative. Hence $N^2 = [24(1 - UN_i(\varepsilon_F))/\mathcal{N}_i''(\varepsilon_F)U^3]$. A moment will form spontaneously at the impurity provided

$$UN_i(\varepsilon_F) > 1. \quad (5.32)$$



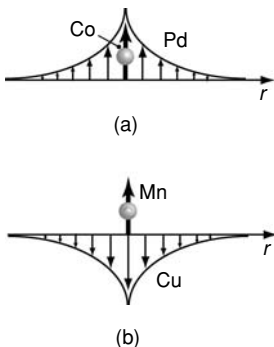
Destruction of an impurity magnetic moment at a critical pressure P_c in the Anderson model.

Since $\mathcal{N}_i(\varepsilon_F)$ is approximately $1/\Delta_i$, we find the Anderson criterion $U \gtrsim \Delta_i$ for magnetism of the impurity. It may be compared with the Stoner criterion for ferromagnetism (5.18). Strong correlations favour magnetism, strong mixing destroys it. If $\mathcal{N}_i(\varepsilon_F)$ varies *smoothly* with some parameter x such as pressure or concentration, then the magnetic moment on the impurity just below the critical value x_c where it disappears will vary as $(x - x_c)^{\frac{1}{2}}$.

The existence of a moment on an atomic site in an alloy may depend sensitively on the local environment. For example, Fe carries a moment when dilute in Mo, but not in Nb. The Fe–Nb hybridization is more effective than Fe–Mo hybridization at broadening the local iron density of states. Iron impurities in $\text{Nb}_{1-x}\text{Mo}_x$ alloys are nonmagnetic when surrounded by less than seven Mo atoms and magnetic when there are seven or more Mo nearest neighbours. In alloys with $x \simeq 0.6$, magnetic and nonmagnetic iron impurities coexist on different sites with different atomic environments. The model where magnetic moments in alloys are governed by the local chemical environment is known as the Jaccarino–Walker model.

Granted a local moment, the s – d Hamiltonian, also known as the Kondo Hamiltonian when \mathcal{J}_{sd} is negative, is written as

$$\mathcal{H} = \sum_{i,j} t_{ij}c_i^\dagger c_j - \sum_{k,l} \mathcal{J}_{sd}\mathbf{S}_k \cdot \mathbf{s}_l. \quad (5.33)$$



(a) A giant moment and (b) a Kondo singlet showing local spin polarization of the host conduction band.

Possible consequences of the interaction between the magnetic impurity and the conduction electrons are the formation of a giant moment when the s – d exchange is ferromagnetic, $\mathcal{J}_{sd} > 0$, or the Kondo effect when the s – d exchange is antiferromagnetic, $\mathcal{J}_{sd} < 0$. The giant moment is due to a cloud of positively polarized electron density surrounding the impurity site. When the paramagnetic susceptibility of the host (5.17) is enhanced beyond the Pauli susceptibility expected from the bare density of states yet not quite sufficiently to meet the Stoner criterion, the dressed local moment can be very large. Cobalt impurities in a palladium host have associated moments of several tens

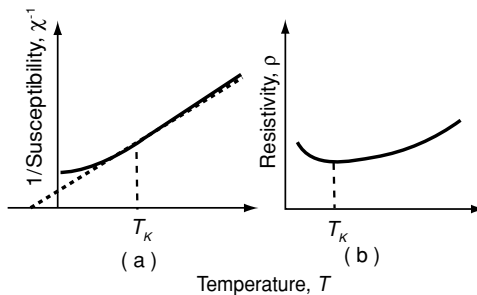
Table 5.3. Kondo temperatures (in kelvin). The host metal is indicated in bold type.

	Cr	Mn	Fe	Co	Ni
Cu	1.0	0.01	25	2000	5000
Ag	.02	.04	3		
Au	0.01	0.01	0.3	200	
Zn	3	1.0	90		
Al	1200	530	5000		

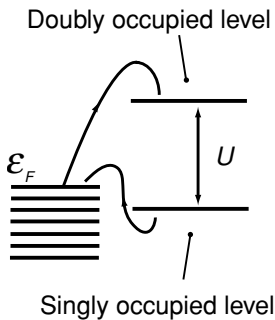
From D. L. Wohlleben and B. R. Coles in *Magnetism 5*, (H. Suhl, editor), New York: Academic Press, 1973.

Figure 5.12

Experimental signs of the Kondo effect: (a) inverse susceptibility of a Kondo alloy and (b) the temperature dependence of the resistivity.



Jun Kondo 1930-.



Kondo scattering. A singlet state is formed between the impurity spin and the conduction electrons.

of Bohr magnetons. There is a threshold beyond which the entire matrix turns ferromagnetic; for Co in Pd, the threshold is only 1.5 at% (see Fig. 10.13(c)).

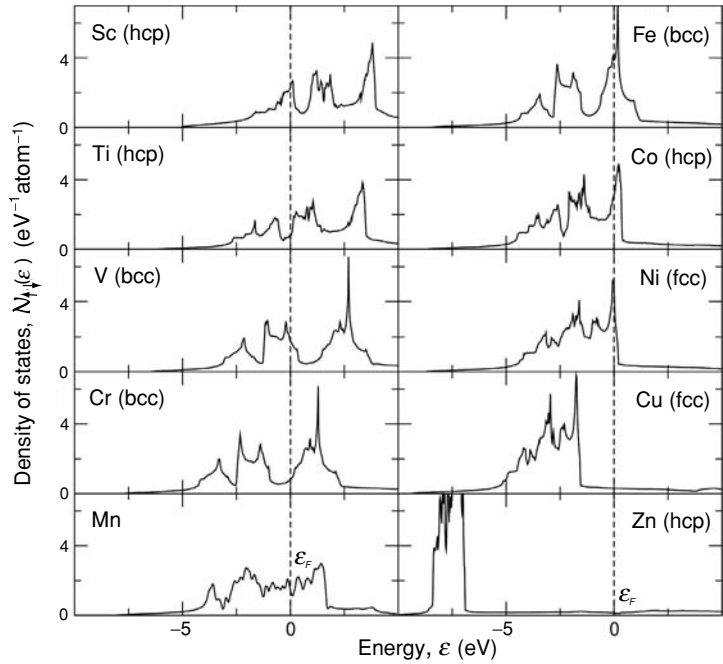
When the exchange coupling between the impurity moment and the conduction electrons \mathcal{J}_{sd} is negative, there is a possibility of forming a nonmagnetic spin singlet state from the impurity and the surrounding cloud of negatively polarized conduction electrons. A good example is iron in copper. The susceptibility is ambiguous; it shows Curie–Weiss temperature dependence (5.7) with negative θ_p above a certain temperature T_K , known as the Kondo temperature, but it becomes temperature-independent below T_K , when the impurity forms a nonmagnetic singlet state with the conduction electrons of the host, Fig. 5.12. According to the system, the Kondo temperature can lie anywhere in the range 1–1000 K. Some values are given in Table 5.3. Another symptom of the Kondo effect is a shallow minimum in the resistivity near T_K , because the Kondo singlets provide an additional channel for scattering conduction electrons. The Kondo temperature is

$$T_K \approx (\Delta_i/k_B) \exp[\Delta_i/2\mathcal{J}_{sd}]$$

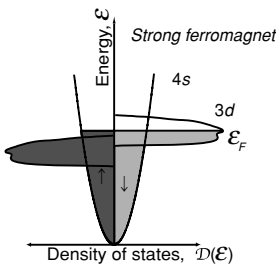
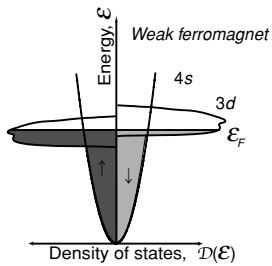
and the excess resistivity due to the Kondo scattering varies logarithmically with temperature; it is proportional to $(\mathcal{J}_{sd}^2/\Delta_i)S(S+1)[1+(2\mathcal{J}_{sd}/\Delta_i)\ln(\Delta_i/k_B T)]$.

Figure 5.13

Densities of states for some metallic elements in the paramagnetic state. Calculations by courtesy of Chaitania Das.



5.3.2 Ferromagnetic metals



Schematic densities of states for a strong and a weak ferromagnet. The $3d^1$ -band is full for the strong ferromagnet.

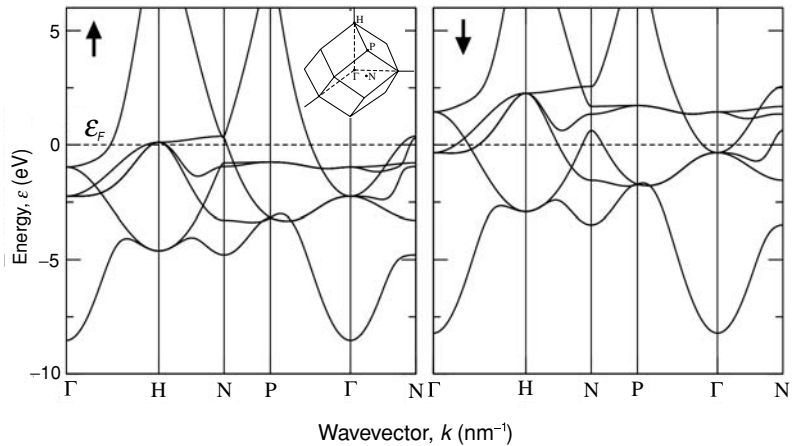
The calculated densities of states for some paramagnetic metals are illustrated in Fig. 5.13. A highly structured $3d$ -band is superposed on a much broader band of $4s$ character. The structure of the d -bands reflects the crystal-field splitting of the t_{2g} - and e_g -bands in 8-fold or 12-fold coordination (Fig. 4.12) in the body-centred cubic (bcc) or face-centred cubic (fcc) structures, as well as the bonding/antibonding splitting between the states near the bottom or the top of the bands, and singularities that appear when the bands cross the boundary of the Brillouin zone.

The band diagrams show the dispersion relations $\epsilon(k)$ of the five d -bands along different directions in k -space in the first Brillouin zone. The Brillouin zone is a primitive unit cell of reciprocal space defined by the Wigner–Seitz procedure, which involves forming the perpendicular bisector planes of the vectors from the origin to neighbouring reciprocal lattice points. The example of iron metal is illustrated in Fig. 5.14. The spin-up and spin-down bands are shown on separate panels. The broad parabolic free-electron-like s -bands, starting at -4 V are barely spin polarized; they hybridize with the d states between -3 and 2 eV for spin-down. The flatter, spin-up d -bands are filled. Two spin-down d bands lie mainly above Fermi level.

In the Stoner picture of metallic ferromagnetism, the bands split spontaneously provided the criterion (5.18) is satisfied. If the splitting is sufficient

Figure 5.14

Spin-polarized energy bands of ferromagnetic α -iron for \uparrow and \downarrow electrons. The majority spin bands are plotted on the left, and the minority spin bands on the right. The points in the Brillouin zone are marked on the insert. The calculated spin moment is $2.2 \mu_B$. (Calculations courtesy of Chaitania Das.)



Edmund Stoner,
1899–1968.

to push the \uparrow d -subband completely below ε_F we have a strong ferromagnet, otherwise we have a weak ferromagnet. Among the ferromagnetic elements, Fe is a weak ferromagnet, but Co and Ni are strong (despite their atomic moments being less than that of iron). In each case there are approximately 0.6 electrons at the bottom of an unsplit sp -band. The $3d$ levels lie above the bottom of the $4s$ -band thanks to the term in the Schrödinger equation for the multielectron atom (4.7) which is identified with orbital kinetic energy. The spin moments of Ni and Co are $0.6 \mu_B$ and $1.6 \mu_B$, respectively. Co has a residual unquenched orbital moment of $0.14 \mu_B$. But that of the other ferromagnets is smaller. Iron would have a spin moment of $2.6 \mu_B$ if it were a strong ferromagnet. In fact, its moment is $2.2 \mu_B$. The calculated spin-split densities of states for Fe, Co and Ni are shown in Fig. 5.15.

The different filling of \uparrow and \downarrow bands leads to different Fermi surfaces for \uparrow and \downarrow electrons. They are illustrated for Fe, Co and Ni in Fig. 5.16. The majority spin surfaces for Co and Ni are quite small and roughly spherical because they contain only electrons with predominantly $4s$ character, whereas Fe has a larger \uparrow Fermi surface. All three have large \downarrow Fermi surfaces.

Table 5.4 summarizes the most important properties of the ferromagnetic $3d$ metals.

Stoner calculated the magnetization as a function of temperature in the free-electron model. His calculation gave an unrealistically high Curie point, $k_B T_C \approx \varepsilon_F$ because the only effect of temperature he considered was the smearing of the Fermi–Dirac occupancy function (3.45) which decreases the density of states near ε_F when $k_B T_C \approx \varepsilon_F$. There should be no band splitting and no moment above T_C . The temperature dependence of the susceptibility above T_C is that given by (3.46). However, in most metallic ferromagnets, T_C is at least an order of magnitude less than predicted by the Stoner theory, and there is a substantial Curie–Weiss-like variation of the susceptibility above T_C . On-site electronic correlations sustain an atomic-scale moment which does not

Figure 5.15

Densities of states for some elements in the ferromagnetic state. Fe is a weak ferromagnet, Co and Ni are strong. Results for γ Fe with different lattice parameters illustrate the sensitivity of the Fe moment to lattice parameter in a dense-packed structure. (Calculations courtesy of Ivan Rungger.)

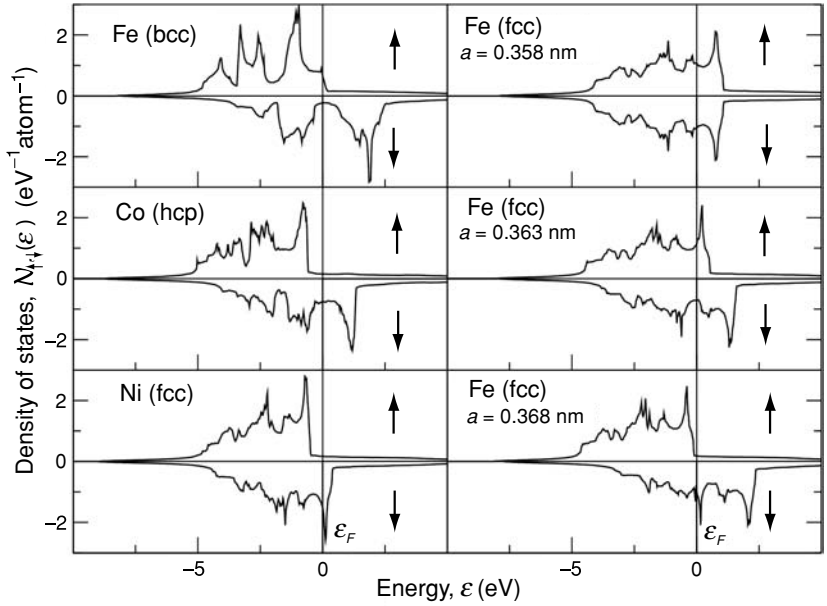


Figure 5.16

The Fermi surfaces of Fe, Co and Ni for \uparrow and \downarrow electrons.

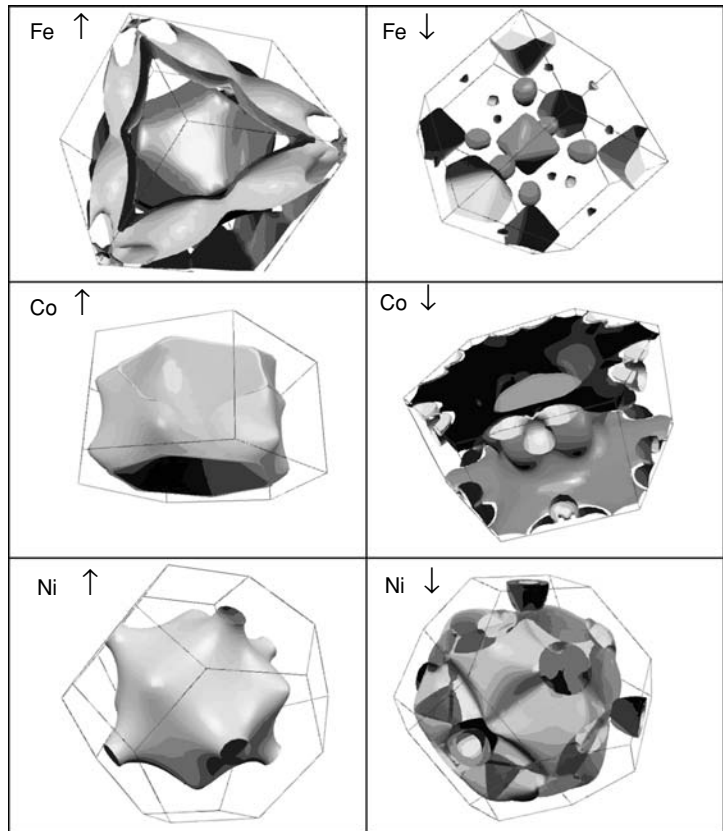


Table 5.4. Intrinsic properties of the ferromagnetic 3d elements at room temperature

T_C (K)	d (kg m^{-3})	σ_s ($\text{A m}^2 \text{ kg}^{-1}$)	M_s (kA m^{-1})	J_s (T)	m (spin/orbit) (μ_B)	$\mathcal{N}_{\uparrow,\downarrow}(\varepsilon_F)$ (eV^{-1})	\mathcal{I} (eV)	K_1 (J m^{-3})	λ_s (10^{-6})	g	D_{sw} (10^{-40} J m^2)
Fe	1044	7874	217	1710	2.15 2.17 (2.09/0.08)	1.54	0.93	48	-7	2.08	4.5
Co	1360(ε)	8920	162(ε)	1440	1.81 1.71 (1.57/0.14)	1.72	0.99	410	-60	2.17	8.0
Ni	628	8902	54.8	488	0.61 0.58 (0.53/0.05)	2.02	1.01	-5	-35	2.18	6.3

Table 5.5. Moments in metallic ferromagnets

		m_{eff}	m_0	T_C
Ni	Strong ferromagnet	1.0	0.6	628
ZrZn ₂	Weak itinerant ferromagnet	1.8	0.2	25
CrO ₂	Half-metal	2.4	2.0	396

disappear at T_C , but becomes disordered in much the same way as it does for the local-moment paramagnet (§4.3) or ferromagnet (§5.1.1). The moment is progressively destroyed by thermal fluctuations when $T \gg T_C$.

Whenever a local moment is disordered but stable in temperature, the effective moment m_{eff} deduced from the susceptibility above T_C using (5.7) should be consistent with the zero-temperature ferromagnetic moment m_0 in the sense of Table 5.5. For metals with nonintegral numbers of unpaired electrons per atom, we can define an effective spin S^* by $2\mu_B S^* = m_0$, and a corresponding effective moment m_{eff} as $2\sqrt{S^*(S^* + 1)}\mu_B$. The Stoner model applies best to some very weak itinerant ferromagnets with $S^* \ll \frac{1}{2}$, such as ZrZn₂, an intermetallic compound of two nonmagnetic elements which exhibits a small ferromagnetic moment and a low Fermi energy. For a weak itinerant ferromagnet, m_{eff} is even larger than expected from this formula. The effect of temperature is not just to destroy the long-range intersite atomic correlations, but also to eliminate progressively the on-site Hund's rule correlations that sustain a local moment. The susceptibility therefore falls more rapidly with increasing temperature than predicted by the Curie–Weiss law.

The rigid-band model envisages a fixed, spin-split density of states for the ferromagnetic 3d elements and their alloys, which is filled up with the necessary number of electrons as if they were water being poured into a jug. The jugs for bcc and fcc metals are differently shaped. Ignoring the small contribution of the 4s-band, the average moment per atom is $\langle m \rangle \approx (N_{3d}^\uparrow - N_{3d}^\downarrow)\mu_B$. The total number of 3d electrons is $N_{3d} = N_{3d}^\uparrow + N_{3d}^\downarrow$, where $N_{3d}^\uparrow = 5$ for the strong ferromagnets. Hence

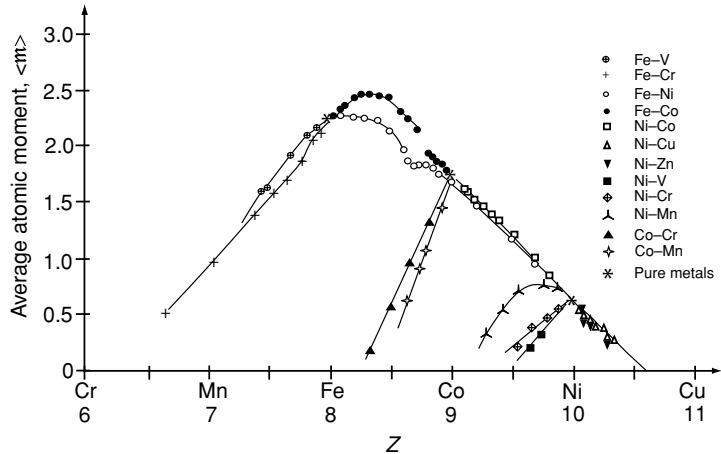
$$\langle m \rangle \approx (10 - N_{3d})\mu_B. \quad (5.34)$$

This relation applies to any strong ferromagnet regardless of the details of the density of states.

The rigid-band picture is oversimplified. Nevertheless, the model has merit. In Cu_xNi_{1-x} alloys, for example, each Cu atom brings an extra electron. The

Figure 5.17

The Slater–Pauling curve. The average atomic moment is plotted against the number of valence ($3d + 4s$) electrons.



d -band of Ni has 0.6 holes and the ferromagnetism of $\text{Cu}_x\text{Ni}_{1-x}$ disappears when the d -band is full up at $x = 0.6$, as predicted.

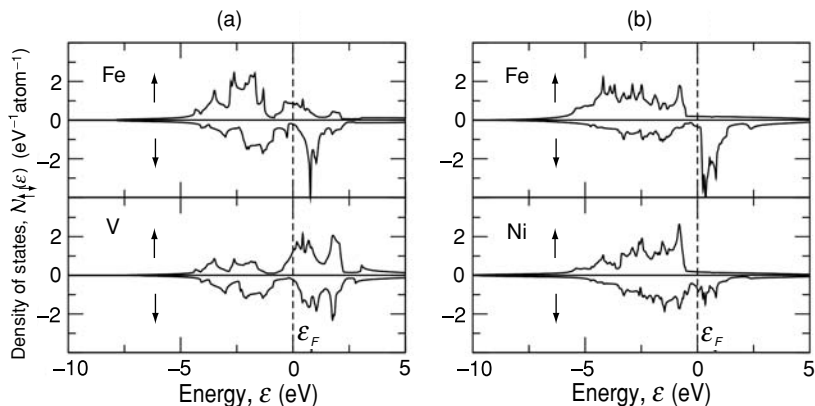
Bonding states with delocalized singlet-like wave functions are found near the bottom of a metallic band and antibonding states with more localized triplet-like states are near the top. Since the total wave function must be antisymmetric, this helps to explain why $3d$ elements near the end of the series tend to be ferromagnetic, while those at the beginning of the series are not. The binding energy of $3d$ electrons increases by about 5 eV across the series, which is comparable to the $3d$ bandwidth. The band narrowing resulting from the increased nuclear charge is sufficient to offset the broadening resulting from reduced metal–metal distances as we move across the $3d$ series.

The famous Slater–Pauling curve, Fig. 5.17, is a plot of the magnetic moment per atom for binary alloys of $3d$ elements plotted against Z , the total number of $3d$ and $4s$ electrons per atom. There is inevitably some mixture of $4p$ character in the $4s$ -band. The alloys on the right-hand side of Fig. 5.17 are strong ferromagnets. The slope of the branch on the right is -1 . The multiple branches with slope ≈ 1 , as expected for rigid bands, are for alloys of late $3d$ elements with early $3d$ elements for which the $3d$ -states lie well above the Fermi level of the ferromagnetic host. The assumption of a common band in the rigid-band model really applies only when the charge difference of the constituent atoms is small, $\Delta Z \lesssim 2$. Otherwise a split band with a joint density of states reflects the densities of states of the constituents. The partial densities of states of FeV and FeNi₃, for example, are compared in Fig. 5.18.

The magnetic valence model is a more general formulation of these ideas which allows us to estimate the average atomic moment per atom of any alloy of a $3d$ element, provided it is a strong ferromagnet. The valence of an atom is given by $\mathcal{Z} = N^\uparrow + N^\downarrow$, where N^\uparrow and N^\downarrow are the numbers of \uparrow and \downarrow valence electrons per atom. The magnetic moment is given by $m = (N^\uparrow - N^\downarrow)\mu_B = (2N^\uparrow - \mathcal{Z})\mu_B$. Now the value of N_d^\uparrow is exactly 5 for strong ferromagnetic

Figure 5.18

Partial densities of states of (a) FeV and (b) FeNi₃.



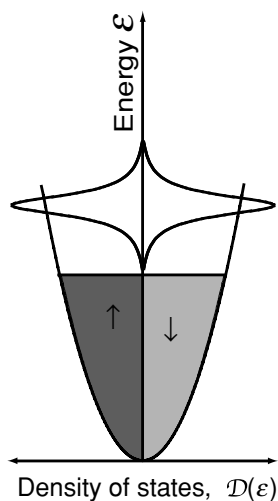
elements, and 0 for main group elements which have no d electrons. The magnetic valence of an element Z_m , defined as

$$Z_m = 2N_d^\uparrow - Z, \quad (5.35)$$

is an integer. Its moment is $m = (Z_m + 2N_s^\uparrow)\mu_B$, where $2N_s^\uparrow \approx 0.6 - 0.7$ is the number of electrons in the unpolarized $4sp$ -band. The average moment per atom in an alloy is obtained by replacing Z_m by its weighted average value over all atoms present in the alloy:

$$\langle m \rangle = (\langle Z_m \rangle + 2N_s^\uparrow)\mu_B. \quad (5.36)$$

In this way it is possible to estimate the magnetization of any strong ferromagnetic alloy based on iron, cobalt or nickel. Some magnetic valences are $Z_m = -3$ for B, Y, La and all rare-earths, -4 for C, Si, Ti, -5 for V, P, -6 for Cr, but 2 for Fe, 1 for Co and 0 for Ni. Taking YFe₂ as an example, the average moment is $[\frac{1}{3}(-3 + 0.6) + \frac{2}{3}(2 + 0.6)] = 0.93 \mu_B/\text{atom}$ or $2.8 \mu_B/(\text{formula unit, fu})$. We can consider that the yttrium has reduced the iron moment from $2.2 \mu_B$ to $1.4 \mu_B$. Adding more yttrium to the alloy will eventually destroy the magnetism entirely (Exercise 5.7(c)). Moments per atom for rare-earth-iron alloys are shown in Fig. 5.19.



A nonmagnetic virtual bound state.

5.3.3 Impurities in ferromagnets

The converse of the problem considered in §5.3.1, the behaviour of a single impurity atom in a ferromagnetic host, is also interesting. If the impurity is a much lighter $3d$ element than the host, like V in Ni (Fig. 5.20) its d levels lie above the Fermi level in the $4s$ conduction band. If V_{kd} is the hopping integral from the d level to the conduction band, the level acquires a width

$$\Delta_i = \pi \mathcal{N}_{4s}(\varepsilon_F) V_{kd}^2, \quad (5.37)$$

Figure 5.19

Variation of the magnetic moment per atom as a function of magnetic valence for some rare-earth iron alloys.

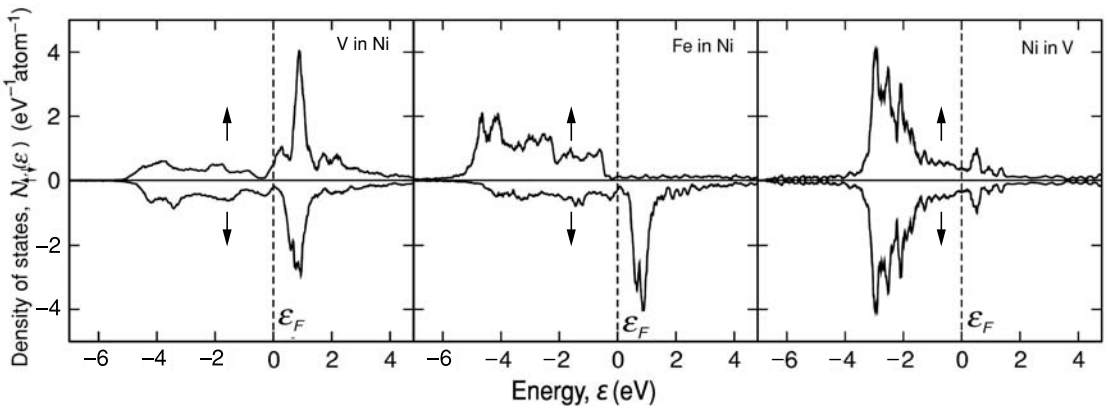
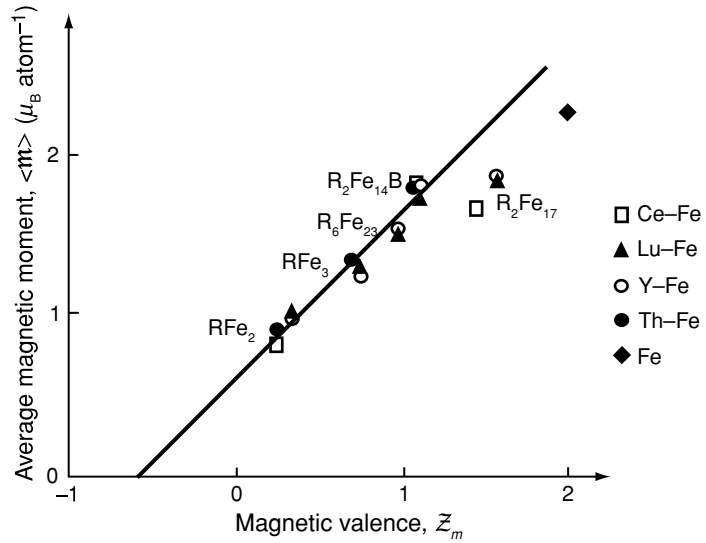


Figure 5.20

The local density of states for V in Ni, Fe in Ni and Ni in V. (Calculations by courtesy of Nadjib Baadji).

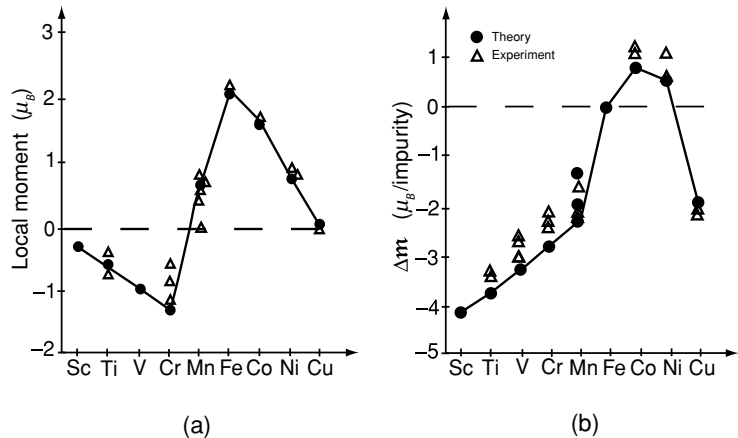
which may be of order 1 eV. The impurity level is then known as a virtual bound state. The width is inversely related to the time an electron dwells on the impurity site.

When the virtual bound state lies entirely above ϵ_F , the $3d$ impurity electrons are emptied into the $3d$ -band of the host. If the host $3d^{\uparrow}$ -band is full, there will be a moment reduction of N_{3d}^i Bohr magnetons, where N_{3d}^i is the number of impurity $3d$ electrons. In addition, the moment of one host atom is suppressed at the site of the substitution. For example, when a V impurity ($Z = 5$, $N_{3d}^i \approx 4$) is substituted in a Ni host, the moment reduction is drastic, $4 + 0.6 = 4.6 \mu_B/\text{V}$.

There will inevitably be some hybridization of the impurity and host $3d$ -states, which will be more effective for the host $3d^{\downarrow}$ electrons, because they lie closer to the Fermi level. A light $3d$ element will therefore acquire a small

Figure 5.21

(a) Local moment carried by 3d impurities in iron, and (b) change of moment per impurity atom substituted into iron (O'Handley, 1999).



(a) $\leftarrow \rightarrow$
 $S_R \quad S_T$

$\rightarrow \rightarrow$

$m_R \quad m_T$

(b) $\leftarrow \rightarrow$
 $S_R \quad S_T$

$\leftarrow \rightarrow$

$m_R \quad m_T$

Coupling of spins and alignment of moments in R-T alloys, T = Fe, Co, Ni (a) R = light rare-earth, (b) R = heavy rare-earth.

negative moment in a heavy 3d host. These trends are illustrated for impurities in iron in Fig. 5.21.

This is an example of the more general rule that *exchange coupling between atoms with d shells that are more than half full with atoms whose d shell is less than half full is antiferromagnetic*. The rare-earths in this context should be considered as light d elements because their atomic configuration is $4f^n 5d^1 6s^2$. There is therefore antiparallel coupling of the *spin* moments of the ferromagnetic 3d elements T = Fe, Co and Ni, and the *spin* moment of a rare-earth. When the 4f shell is half-filled, or more, this leads to *antiparallel* coupling of the atomic moments in R-T alloys with R = Gd-Yb. However, in light rare-earth metals where the moment is mainly orbital in character, and directed opposite to the spin moment according to Hund's third rule, the R and T moments are *parallel*, even though the spins are antiparallel. Many examples of R-T alloys are presented in Chapter 11.

5.3.4 Half-metals

These oddly named materials are ferromagnets with electrons of only one spin polarization at the Fermi level. Cobalt and nickel are *not* half-metals because of the presence of the 4s electrons at ϵ_F which are not fully spin-polarized. Indeed, no ferromagnetic element is a half-metal. It is necessary to form a compound where the 4s electrons can be removed from the vicinity of the Fermi energy by charge transfer or hybridization. Examples include the oxide CrO_2 and the ordered intermetallic compound MnNiSb , which are both discussed in Chapter 11. The characteristic feature of a half-metal is a spin gap in the \uparrow or \downarrow density of states at ϵ_F . Furthermore, the spin moment per formula unit in a stoichiometric half-metallic compound is an *integral number of Bohr magnetons*. This is because there are an integral number $N^\uparrow + N^\downarrow$ of electrons per formula unit,

and the band with the spin gap must contain an integral number of N^\uparrow (or N^\downarrow) electrons, hence $N^\uparrow - N^\downarrow$ is also an integer.

Spin-orbit interaction tends to destroy half-metallicity by mixing \uparrow and \downarrow states, as explained in §5.6.4.

5.3.5 The two-electron model

Further insight into the physical interactions of importance in metals is provided by a diatomic two-electron model. Although highly simplified, the model contains most of the ingredients of the physics of the many-electron problem, except orbital degeneracy. Important quantities are the on-site Coulomb repulsion U , the transfer or ‘hopping’ integral t which gives rise to the bandwidth W and the direct exchange \mathcal{J}_d .

The Hamiltonian $\mathcal{H}(\mathbf{r}_1, \mathbf{r}_2)$ is that in the Schrödinger equation of (5.20), with an additional term $e^2/4\epsilon_0 |\mathbf{r}_1 - \mathbf{r}_2|$ to take account of the Coulomb interaction of the two electrons with each other. The spatially symmetric and antisymmetric wave functions

$$\phi_s = (1/\sqrt{2})(\psi_1 + \psi_2), \quad \phi_a = (1/\sqrt{2})(\psi_1 - \psi_2), \quad (5.21)$$

may be regarded as embryonic Bloch functions (electron waves) for the metal with $k = 0$ and $k = \pi/d$, where d is the interatomic spacing. We can replace ϕ_s and ϕ_a by embryonic Wannier functions which are mostly localized on the left and right atoms:

$$\phi_l = (1/N)(\psi_1 + a\psi_2), \quad \phi_r = (1/N)(a\psi_1 + \psi_2), \quad (5.38)$$

with

$$a = \frac{-1 + \sqrt{1 - \mathcal{S}^2}}{\mathcal{S}},$$

where \mathcal{S} is the overlap integral $\int \psi_1^*(r)\psi_2(r)d^3r$ and N is a normalization factor. These Wannier functions, Fig. 5.22, differ from ψ_1 and ψ_2 , the eigenfunctions of the one-electron problem, in that they are supposed to be orthogonal $\int \phi_l^*(r)\phi_r(r)d^3r = 0$.

There are now four possible two-electron wave functions $\Psi_i(\mathbf{r}, \mathbf{r}')$:

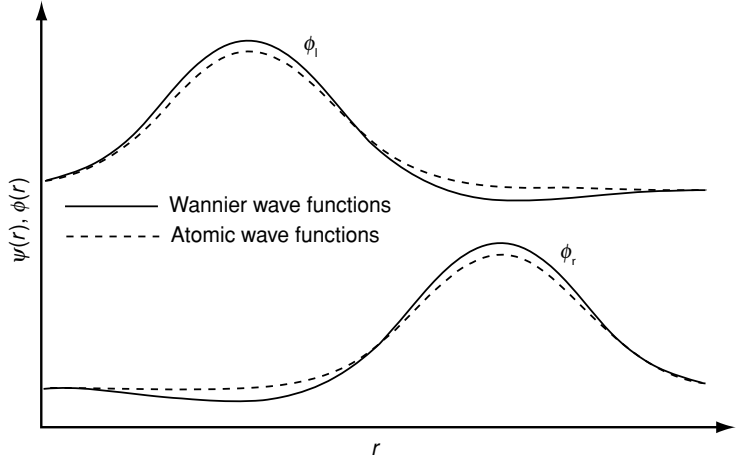
$$\begin{aligned} \Psi_1 &= \phi_l(\mathbf{r})\phi_l(\mathbf{r}'); & \Psi_2 &= \phi_l(\mathbf{r})\phi_r(\mathbf{r}'); \\ \Psi_3 &= \phi_r(\mathbf{r})\phi_l(\mathbf{r}'); & \Psi_4 &= \phi_r(\mathbf{r})\phi_r(\mathbf{r}'). \end{aligned}$$

The functions Ψ_1 and Ψ_4 represent doubly occupied states. The interaction matrix is

$$\begin{pmatrix} U & t & t & \mathcal{J}_d \\ t & 0 & \mathcal{J}_d & t \\ t & \mathcal{J}_d & 0 & t \\ \mathcal{J}_d & t & t & U \end{pmatrix}. \quad (5.39)$$

Figure 5.22

Wannier functions and atomic wave functions for the diatomic molecule.



The Coulomb interaction U is the energy penalty when two electrons are put into the same orbital. It is several electron volts:

$$U = \int \phi_l^*(\mathbf{r})\phi_l^*(\mathbf{r}')\mathcal{H}(\mathbf{r}, \mathbf{r}')\phi_l(\mathbf{r})\phi_l(\mathbf{r}')d^3r d^3r'.$$

The transfer or hopping integral t is also positive, and is $\lesssim 1$ eV. It represents the bandwidth. More generally, in the tight-binding approximation, the bandwidth is $2Z_n t$, where Z_n is the number of nearest neighbours.

$$t \approx \int \phi_R^*(\mathbf{r})\phi_l^*(\mathbf{r}')\mathcal{H}(\mathbf{r}, \mathbf{r}')\phi_l(\mathbf{r})\phi_r(\mathbf{r}')d^3r d^3r'$$

The direct exchange between doubly occupied sites is smaller, and of order 0.1 eV:

$$\mathcal{J}_d = \int \phi_l^*(\mathbf{r})\phi_l^*(\mathbf{r}')\mathcal{H}(\mathbf{r}, \mathbf{r}')\phi_r(\mathbf{r})\phi_r(\mathbf{r}')d^3r d^3r'.$$

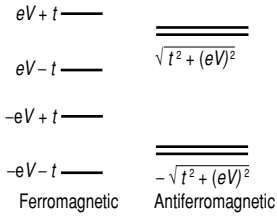
The interaction matrix (5.39) can be diagonalized directly. Two doubly occupied states have eigenvalues of order U , and are therefore neglected. The other states, which are much lower in energy, are: (i) a delocalized ferromagnetic state (the spatial part of the wave function is antisymmetric) with eigenvalue $\varepsilon_{FM} = -\mathcal{J}_d$

$$\Psi_{FM} = (1/\sqrt{2})[\phi_l(\mathbf{r})\phi_r(\mathbf{r}') - \phi_r(\mathbf{r})\phi_l(\mathbf{r}')];$$

and (ii) an antiferromagnetic state (the spatial part of the wave function is symmetric)

$$\begin{aligned} \Psi_{AF} = & (\sin \chi/\sqrt{2})[\phi_l(\mathbf{r})\phi_l(\mathbf{r}') + \phi_r(\mathbf{r})\phi_r(\mathbf{r}')] \\ & + (\cos \chi/\sqrt{2})[\phi_l(\mathbf{r})\phi_r(\mathbf{r}') + \phi_r(\mathbf{r})\phi_l(\mathbf{r}')], \end{aligned}$$

where $\tan \chi = 4t/U$. The associated energy is $\varepsilon_{AF} = U/2 + \mathcal{J}_d - \sqrt{4t^2 + U^2/4}$.



Energy levels of the ferromagnetic and antiferromagnetic states for the two-atom/ four-state problem.

The effective exchange is $\mathcal{J}_{eff} = \frac{1}{2}(\varepsilon_{AF} - \varepsilon_{FM})$,

$$\mathcal{J}_{eff} = \mathcal{J}_d + U/4 - \sqrt{(t^2 + U^2/16)}. \quad (5.40)$$

$\mathcal{J}_{eff} > 0$ indicates a ‘ferromagnetic’ ground state and $\mathcal{J}_{eff} < 0$ indicates an ‘antiferromagnetic’ ground state. Direct exchange favours ferromagnetism, but strong interatomic hopping t favours antiferromagnetism. When $U \gg t$, and $\mathcal{J}_d = 0$, the exchange is antiferromagnetic, as illustrated in §5.2.2:

$$\mathcal{J}_{eff} = -2t^2/U. \quad (5.41)$$

Our rudimentary model can also illustrate how exchange depends on band filling. We consider the ferromagnetic and the antiferromagnetic states, for which the one-electron Hamiltonians are,

$$\mathcal{H}_F = \begin{bmatrix} \pm eV & t \\ t & \pm eV \end{bmatrix},$$

$$\mathcal{H}_{AF} = \begin{bmatrix} \pm eV & t \\ t & \mp eV \end{bmatrix},$$

where V is the local exchange potential experienced by an electron on site 1 or 2 and t is the interatomic hopping integral. When $t = 0$, there is one-electron exchange splitting of the states. Diagonalizing the matrices to find the eigenvalues involves solving the determinant $|\mathcal{H} - \lambda\mathbf{I}| = 0$. For the ferromagnetic state, the energy levels are $\pm eV + t$ and $\pm eV - t$, whereas for the antiferromagnetic state, they are doubly degenerate $\pm\sqrt{t^2 + (eV)^2}$. It can be seen that a single electron or three electrons (quarter-filled or three-quarters-filled band) go into a ferromagnetic state, but two electrons (half-filled band) prefer the antiferromagnetic state.

5.3.6 The Hubbard model

A famous model Hamiltonian which represents electron correlation in the tight-binding model for an array of one-electron atoms is

$$\mathcal{H} = - \sum_{i,j} t c_i^\dagger c_j + U \sum_i N_i^\uparrow N_i^\downarrow,$$

where $N_i^{\uparrow,\downarrow}$ are the numbers of spin-up and spin-down electrons, respectively, on the i th atom. The first term is the transfer term that creates the band of width $W = 2Zt$; the second is the Coulomb energy penalty involved in placing two electrons on the same atom.

Electrons are localized when $U/W > 1$ because there are then no states available to accommodate the double-occupancy charge fluctuations that are indispensable for electronic conduction. Compounds with an integral number of electrons per atom which satisfy this condition are known as Mott-Hubbard insulators.

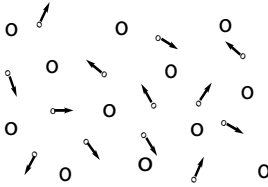
The second term can be rewritten using

$$UN_i^\uparrow N_i^\downarrow = U[(N^\uparrow + N^\downarrow)^2/4 - (N^\uparrow - N^\downarrow)^2/4].$$

The Stoner interaction $-(\mathcal{I}/4)(N^\uparrow - N^\downarrow)^2$ is thereby identified as the spin-dependent part of the on-site Coulomb interaction; hence $\mathcal{I} \approx U$. In the Hubbard model, the on-site correlations create a magnetic moment, and hopping between adjacent nondegenerate singly occupied orbitals provides an antiferromagnetic interaction.

A variant of the Hubbard model is the t - \mathcal{J} model, where the second term is replaced by $-2\mathcal{J} \sum_{i>j} \mathbf{S}_i \cdot \mathbf{S}_j$ with $\mathcal{J} = -2t^2/U$.

5.3.7 Electronic structure calculations



The Born-Oppenheimer approximation: the electrons (marked with arrows) move in a background of frozen nuclei (open circles).

A solid is a system of N electrons at positions $\{\mathbf{r}_i\}$ and N' nuclei, usually centred on a periodic lattice $\{\mathbf{R}_I\}$. Inner electrons occupy tightly bound, localized core orbitals around the nuclei. Outer orbitals with binding energies of a few electron volts or less are the home of the valence and conduction electrons, which determine the electronic character of the solid, be it metal, semiconductor, insulator, ferromagnet, antiferromagnet, superconductor, . . . The instantaneous velocity of these outer electrons is of order the Fermi velocity, $v_F \approx 10^6 \text{ m s}^{-1}$. Ion cores vibrate at phonon frequencies that are of order 10^{14} Hz , with an amplitude of about 10 pm, which means that their velocity is of order 10^3 m s^{-1} . We are therefore justified in thinking that the electron sees the potential of a set of nuclei instantaneously frozen in position – the Born-Oppenheimer approximation. Furthermore, we will ignore the atomic displacements, which lead to electron scattering, and assume that the ion cores are localized at the lattice sites. The electrons experience Coulomb interactions with the nuclei, and with each other. The Hamiltonian, with factors of $\frac{1}{2}$ to avoid double counting, takes the form

$$\mathcal{H} = - \sum_i \frac{\hbar^2 \nabla_i^2}{2m_e} - \sum_{i,I} \frac{Ze^2}{4\pi\epsilon_0 R_{Ii}} + \frac{1}{2} \sum_{i,j} \frac{e^2}{4\pi\epsilon_0 r_{ij}}. \quad (5.42)$$

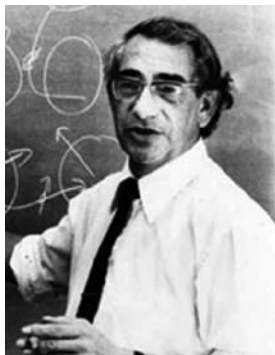
The problem is to solve Schrödinger's equation $\mathcal{H}\Psi = \epsilon\Psi$, where $\Psi(\{\mathbf{R}_I\}, \{\mathbf{r}_i\})$ is a wave function for the huge number of electrons and nuclei in the system.

An abbreviated notation for \mathcal{H} is

$$\mathcal{H} = \mathcal{T} + \mathcal{V} + \mathcal{U}, \quad (5.43)$$

where \mathcal{T} and \mathcal{V} are the terms corresponding to the one-electron kinetic and potential energy and \mathcal{U} represents the two-electron interactions that capture the complexity of the physics.

Many first-principles methods for solving the many-electron Schrödinger equation use wave functions based on Slater determinants. The idea is to build in the antisymmetry of the wave function under exchange of any two electrons



John Hubbard, 1931–1980

with given space and spin coordinates x, y, z, σ denoted as \mathbf{x}_i and \mathbf{x}_j . In the case of just two electrons, for example, $\Psi = \psi_1(\mathbf{x}_1)\psi_2(\mathbf{x}_2)$ is not antisymmetric, but $(1/\sqrt{2})[\psi_1(\mathbf{x}_1)\psi_2(\mathbf{x}_2) - \psi_1(\mathbf{x}_2)\psi_2(\mathbf{x}_1)]$ is a suitable wave function. It can be written in the form of a determinant:

$$\Psi(\mathbf{x}_1, \mathbf{x}_2) = \frac{1}{\sqrt{2}} \begin{vmatrix} \psi_1(\mathbf{x}_1) & \psi_2(\mathbf{x}_1) \\ \psi_1(\mathbf{x}_2) & \psi_2(\mathbf{x}_2) \end{vmatrix}. \quad (5.44)$$

Placing two electrons in the same orbit $\psi_1 = \psi_2$ gives $\Psi(\mathbf{x}_1, \mathbf{x}_2) = 0$, as required by the Pauli principle. Slater generalized this idea to N electrons, writing the wave function as

$$\Psi(\mathbf{x}_1, \mathbf{x}_2, \dots, \mathbf{x}_N) = \frac{1}{\sqrt{N!}} \begin{vmatrix} \psi_1(\mathbf{x}_1) & \psi_2(\mathbf{x}_1) & \dots & \psi_N(\mathbf{x}_1) \\ \psi_1(\mathbf{x}_2) & \psi_2(\mathbf{x}_2) & \dots & \psi_N(\mathbf{x}_2) \\ \vdots & \vdots & \ddots & \vdots \\ \psi_1(\mathbf{x}_N) & \psi_2(\mathbf{x}_N) & \dots & \psi_N(\mathbf{x}_N) \end{vmatrix}. \quad (5.45)$$

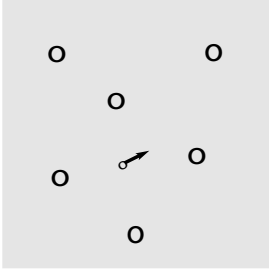
A compact way to denote a Slater determinant is as a ket, $|1, 2, \dots, N\rangle$.

The Hartree–Fock method assumes that the exact N -electron wave function of the system can be approximated as a single Slater determinant. A variational solution is then based on a linear combination of these one-electron wave functions with coefficients chosen to minimize the energy. The method completely neglects electron correlations, but takes perfect account of the exchange. Each electron is surrounded by an exchange hole, from which any other electron with the same spin is excluded.

An alternative approach to Hartree–Fock calculations is density functional theory (DFT), which provides an approximate solution for both exchange and correlation energies. It succeeds in mapping a many-electron problem with \mathcal{U} onto a one-electron problem without \mathcal{U} . The theory is based on two theorems, proved by Hohenberg and Kohn in the mid 1960s. The first is that *the density $n(\mathbf{r})$ of a system of N electrons determines all the ground-state electronic properties*. The ground-state wave function Ψ_0 is a unique functional of electron density $\Psi_0[n(\mathbf{r})]$. (A functional is just a function which has another function as its argument.) Other physical properties can be derived from the wave function. In particular, the ground-state energy is

$$\varepsilon_0[n(\mathbf{r})] = \langle \Psi_0 | \mathcal{T} + \mathcal{V} + \mathcal{U} | \Psi_0 \rangle. \quad (5.46)$$

The second is that *the energy functional $\varepsilon_0[n(\mathbf{r})]$ is lower in energy for the ground-state density $n_0(\mathbf{r})$ than any other state*. The term in the energy which needs to be minimized in (5.46) is the one that depends on $\{R_I\}$, $\mathcal{V}[n(\mathbf{r})] = -e \int V(\mathbf{r})n(\mathbf{r})d^3r$. The significance of these theorems is that it is immensely easier to base a calculation on the density, which depends on only three variables, x, y, z , or four when we include the spin σ , than it is on the wave functions of an N -electron system which depend on $4N$ variables. The problem is that the correct density functional is unknown, and it must be arrived at by inspired approximation. Furthermore, the method applies to the ground state,



The Kohn-Sham formalism. Each electron moves independently in an effective potential created by the others.

and it does not give the structure of excited states, although a time-dependent variant of the theory may remedy this defect.

Density functional theory is usually implemented using the Kohn-Sham method, where the problem of strongly interacting electrons moving in the potential of the nuclei is reduced to the more tractable problem of noninteracting electrons in an effective potential which somehow takes care of the inter-electronic Coulomb interaction, as well as exchange and correlation effects. The energy of (5.46) is rewritten as

$$\varepsilon_0[n(\mathbf{r})] = T_s[n(\mathbf{r})] + \varepsilon_V[n(\mathbf{r})], \quad (5.47)$$

where T_s is the noninteracting kinetic energy and ε_V is the total potential energy. The Kohn-Sham equations for this noninteracting system are just a set of effective, single-particle Schrödinger equations

$$\left[-\frac{\hbar^2 \nabla_i^2}{2m_e} + \mathcal{V}_s(\mathbf{r}) \right] \phi_i(\mathbf{r}) = \varepsilon_i \phi_i(\mathbf{r}) \quad (5.48)$$

which yield a set of orbitals ϕ_i which are approximate wave functions for the real system of electrons that reproduce the density of the original many-electron system $n(\mathbf{r}) = \sum_i |\phi_i^2|$. The effective single-particle potential is usually written as

$$\mathcal{V}_s = \mathcal{V} + \frac{1}{2} \int \frac{e^2 n(\mathbf{r}')}{4\pi \epsilon_0 |\mathbf{r} - \mathbf{r}'|} d^3 r' + \mathcal{V}_{xc}[n(\mathbf{r})]. \quad (5.49)$$

The first term is the Coulomb interaction of the electron with the nuclei, the second term is the Hartree term \mathcal{V}_H describing the electron-electron Coulomb repulsion, and the key term is the third one, the exchange-correlation potential, which includes all the many-electron correlations. The Kohn-Sham equations are solved by following an iterative procedure. Taking an initial guess for $[n(\mathbf{r})]$, \mathcal{V}_s is calculated and the equations are solved for $\phi_i(\mathbf{r})$, from which a new density is calculated, and the process is repeated. The local density approximation (LDA) assumes that the exchange-correlation functional $\mathcal{V}_{xc}[n\{\mathbf{r}\}]$ depends only on the density at the point where the function is evaluated $\mathcal{V}_{xc}[n(\mathbf{r})]$. A variant is the general gradient approximation, where \mathcal{V}_{xc} depends also on the density gradient $\mathcal{V}_{xc}[n(\mathbf{r}), \nabla n(\mathbf{r})]$. In systems of more ionic character, a U term can be added to reduce double orbital occupancy.

All this can be generalized to the spin-dependent case. In the local spin density approximation (LSDA) two densities must be taken into account, the scalar electron density $n(\mathbf{r})$ and the vector magnetization density $\mathbf{m}(\mathbf{r}) = \mu_B [n^\uparrow(\mathbf{r}) - n^\downarrow(\mathbf{r})] \mathbf{e}_z$. They are both incorporated in a 2×2 density matrix $\hat{\mathbf{n}}(\mathbf{r}) = \frac{1}{2} [n(\mathbf{r}) \hat{\mathbf{1}} + \hat{\boldsymbol{\sigma}} \cdot \mathbf{s}(\mathbf{r})]$, where $\hat{\mathbf{1}}$ is the identity matrix $\begin{bmatrix} 1 & 0 \\ 0 & 1 \end{bmatrix}$, $\hat{\boldsymbol{\sigma}}$ are the Pauli spin matrices (3.17) and $\mathbf{s}(\mathbf{r})$ is the local spin density $\mathbf{m}(\mathbf{r})/\mu_B$. For a

collinear spin configuration, the density matrix is diagonal:

$$\hat{\mathbf{n}}(\mathbf{r}) = \begin{bmatrix} n^\uparrow(\mathbf{r}) & 0 \\ 0 & n^\downarrow(\mathbf{r}) \end{bmatrix}, \quad (5.50)$$

so that $n(\mathbf{r}) = n^\uparrow(\mathbf{r}) + n^\downarrow(\mathbf{r})$ and $\mathbf{m}(\mathbf{r}) = \mu_B [n^\uparrow(\mathbf{r}) - n^\downarrow(\mathbf{r})]$. The potential matrix is given by $\hat{\mathcal{V}} = \mathcal{V}\hat{\mathbf{I}} + \mu_B \mathbf{m}(\mathbf{r}) \cdot \mathbf{B}$, where \mathbf{B} is the magnetic field. The spin-polarized version of the Kohn–Sham equations is

$$\left[\left(-\frac{\hbar^2 \nabla_i^2}{2m_e} + \mathcal{V}_H \right) \hat{\mathbf{I}} + \mathcal{V} + \mathcal{V}_{xc} \right] \begin{bmatrix} \phi_i^\uparrow(\mathbf{r}) \\ \phi_i^\downarrow(\mathbf{r}) \end{bmatrix} = \varepsilon_i \begin{bmatrix} \phi_i^\uparrow(\mathbf{r}) \\ \phi_i^\downarrow(\mathbf{r}) \end{bmatrix}. \quad (5.51)$$

The exchange-correlation matrix depends on both $n(\mathbf{r})$ and $\mathbf{m}(\mathbf{r})$,

$$\mathcal{V}_{xc} = \mathcal{V}_{xc}[n(\mathbf{r}), \mathbf{m}(\mathbf{r})], \quad (5.52)$$

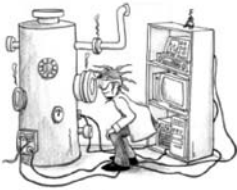
for which a suitable approximation must be found. Equations (5.51) yield the wave functions $\phi_i^{\uparrow,\downarrow}(\mathbf{r})$ from which the density matrix $\hat{\mathbf{n}}(\mathbf{r})$ is deduced. A self-consistent solution is obtained, as in the nonmagnetic case. A number of computer codes are available to do the job. If the density matrix is diagonal, the magnetic structure is collinear, but the general formalism allows for noncollinear structures. DFT is an accurate method for calculating magnetic moments and spin-polarized band structures, especially in metallic systems.

Exponential growth of computer power, and especially multiprocessor computer clusters, has enabled computer simulation to establish itself as a third force, alongside experiment and theory, for investigations in magnetism. Not only in electronic structure calculations, where it is becoming possible to investigate the crystal structure and magnetic order of a new compound without ever actually having to make it in the laboratory, but also in the areas of electronic transport properties and micromagnetism, are computational methods making their mark. Large numbers of atoms, of order 1000 or more, can be handled using current DFT codes, which makes it possible to investigate spin-dependent transport in a molecule, or to study the appearance of a magnetic moment on different types of lattice defects in a solid. It is immensely more convenient to create a specific complex lattice defect on a computer than it is in the laboratory.

5.4 Collective excitations

The comparison of magnetization data on nickel with the predictions of molecular field theory for $J = \frac{1}{2}$ in Fig. 5.3 shows discrepancies both at low temperature, and in the vicinity of T_C . Actually the discrepancies are worse than they appear because T_C is used to determine n_W , so the model is constrained to return the right Curie temperature, and the correct value of m_0 .

Experimental methods discussed in Chapter 10, exist to determine the exchange constants directly, so it is possible to make a more telling comparison



The three forces in magnetism: theory, experiment, and simulation. (Courtesy Wiebke Drenckhan).

Figure 5.23

Spontaneous magnetization and inverse susceptibility as a function of temperature. The molecular field predictions (grey) are compared with typical experimental data (black).

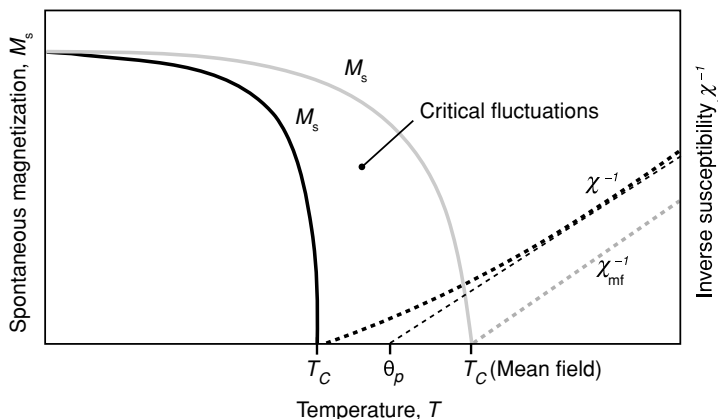
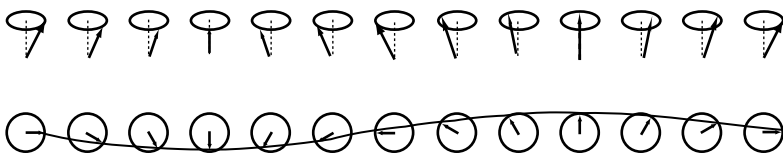


Figure 5.24

Illustration of a spin wave.



between theory and experiment, as indicated in Fig. 5.23. Here it is evident that ferromagnetism is considerably less stable at elevated temperature than molecular field theory would have us believe; it overestimates T_C by as much as a factor of 2, depending on the dimensions and the lattice type. The spontaneous magnetization is diminished at low temperatures by spin-wave excitations. Near T_C the critical fluctuations destroy it.

5.4.1 Spin waves

The total exchange energy in the ferromagnetic ground state is $-2Z\mathcal{J}S^2$ per site, where Z is the number of magnetic nearest neighbours and \mathcal{J} is the nearest-neighbour exchange interaction. The elementary excitations from the ferromagnetic ground state are not, as might be imagined, flips of individual spins that reduce an atomic moment from a state with $M_s = S$ to one with $M_s = (S - 1)$. A single localized spin reversal in an $S = \frac{1}{2}$ chain $\uparrow\uparrow\uparrow\downarrow\uparrow\uparrow\uparrow$ costs $8\mathcal{J}S^2$ or $2\mathcal{J}$ when $S = \frac{1}{2}$, which is twice as large as $k_B T_C$ for the chain treated in the molecular field approximation (5.26); $Z = 2$ for a chain, so $k_B T_C = 2\mathcal{J}ZS(S + 1)/3 = \mathcal{J}$. Such expensive excitations cannot occur at low temperature. Instead, all the atoms share out the spin reversal, with periodic oscillation of their transverse spin orientation. The spin deviations spread over the whole lattice in a propagating spin wave with wave vector \mathbf{q} and energy $\varepsilon_q = \hbar\omega_q$, as illustrated in Fig. 5.24. Spin waves exist as classical excitations, but the extended, quantized spin deviations in solids are known as magnons by analogy with phonons, the quantized lattice waves. Think of spin waves

as oscillations in the relative orientations of spins on a lattice, whereas lattice waves are oscillations of the relative positions of atoms on a lattice.

The relation between the wavevector $q = 2\pi/\lambda$ and frequency ω_q of the spin wave can be calculated classically, or from quantum mechanics. The classical approach considers the spin angular momentum of the atom at site j , $\hbar\mathbf{S}_j$ and equates the torque exerted by the molecular field to the rate of change of angular momentum, thus

$$\hbar \frac{d\mathbf{S}_j}{dt} = \mu_0 g \mu_B \mathbf{S}_j \times \mathbf{H}^j. \quad (5.53)$$

In a chain, the molecular field \mathbf{H}^j at site j is due to the neighbours at sites $j \pm 1$. From (5.25), $\mathbf{H}^j = 2\mathcal{J}(\mathbf{S}_{j-1} + \mathbf{S}_{j+1})/\mu_0 g \mu_B$, hence $\hbar d\mathbf{S}_j/dt = 2\mathcal{J}\mathbf{S}_j \times (\mathbf{S}_{j-1} + \mathbf{S}_{j+1})$. This can be written in Cartesian coordinates:

$$\hbar \frac{dS_j^x}{dt} = 2\mathcal{J}[S_j^y(S_{j-1}^z + S_{j+1}^z) - S_j^z(S_{j-1}^y + S_{j+1}^y)]$$

plus cyclic permutations. For small deviations, we can approximate $S_j^z = S_j = S$ and neglect terms like $S_i^x S_j^y$. Hence

$$\begin{aligned} \hbar \frac{dS_j^x}{dt} &= 2\mathcal{J}S[2S_j^y - S_{j-1}^y - S_{j+1}^y], \\ -\hbar \frac{dS_j^y}{dt} &= 2\mathcal{J}S[2S_j^x - S_{j-1}^x - S_{j+1}^x], \\ \hbar \frac{dS_j^z}{dt} &= 0. \end{aligned} \quad (5.54)$$

Solutions are of the form $S_j^x = uS \exp[i(jqa - \omega_q t)]$, $S_j^y = vS \exp[i(jqa - \omega_q t)]$, where q is the wavevector and a is the interatomic spacing. Substituting back into (5.54) gives $-i\hbar\omega_q u = 4\mathcal{J}S(1 - \cos qa)v$, $i\hbar\omega_q v = 4\mathcal{J}S(1 - \cos qa)u$. Multiplying these results for a one-dimensional chain of isotropic spins, gives

$$\hbar\omega_q = 4\mathcal{J}S(1 - \cos qa). \quad (5.55)$$

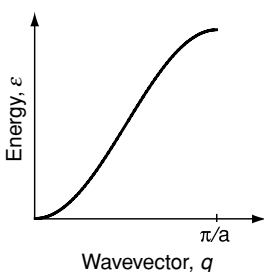
In the limit of small wavevectors, the spin-wave dispersion relation becomes

$$\varepsilon_q \approx D_{sw} q^2, \quad (5.56)$$

where $\varepsilon_q = \hbar\omega_q$ and the spin-wave stiffness parameter is $D_{sw} = 2\mathcal{J}Sa^2$. It takes a vanishingly small energy to create a long-wavelength magnetic excitation. The generalization to a three-dimensional cubic lattice with nearest-neighbour interactions is

$$\hbar\omega_q = 2\mathcal{J}S \left[Z - \sum_{\delta} \cos \mathbf{q} \cdot \boldsymbol{\delta} \right],$$

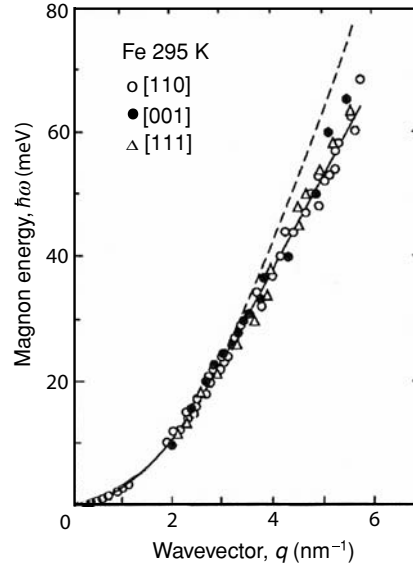
where the sum is over the Z vectors $\boldsymbol{\delta}$ connecting the central atom to its nearest neighbours. The same dispersion relation with $D_{sw} = 2\mathcal{J}Sa_0^2$ is found in any of



The spin-wave dispersion relation for a chain of atoms.

Figure 5.25

The magnon dispersion relations for iron measured in different directions in the unit cell. The dashed line corresponds to $D_{sw} = 4.5 \times 10^{-40} \text{ J m}^2$. (G. Shirane *et al.*, *Journal of Applied Physics*, **39**, 383 (1968))



the three basic cubic lattices, where a_0 is now the lattice parameter. Dispersion of magnons differs from that of phonons, $\varepsilon_q \approx c_0 q$ where c_0 is the velocity of sound, which is linear in the small- q limit. The value of D_{sw} for cobalt, for example, is $8.0 \times 10^{-40} \text{ J m}^2$ (500 meV \AA^2). It is smaller for other ferromagnets (Table 5.4). The dispersion relation for iron is shown in Fig. 5.25.

Equation (5.55) can be derived quantum mechanically from the Heisenberg Hamiltonian (5.24) where the sum is over nearest-neighbour pairs i, j . The Hamiltonian

$$\mathbf{S}_i \cdot \mathbf{S}_j = S_i^x S_j^x + S_i^y S_j^y + S_i^z S_j^z \quad (5.57)$$

is written in terms of the raising and lowering operators.

$$\mathbf{S}_i \cdot \mathbf{S}_j = S_i^z S_j^z + \frac{1}{2}(S_i^+ S_j^- + S_i^- S_j^+). \quad (5.58)$$

The ground state of the system $|\Phi\rangle$ has all the spins aligned in the z -direction, so that $\mathcal{H}|\Phi\rangle = -2\mathcal{J}(N-1)S^2|\Phi\rangle$. Flipping a spin $\frac{1}{2}$ at site i using S_i^- reduces M_S^z from S to $S-1$; $|i\rangle = S_i^-|\Phi\rangle$ lowers the total spin of the system by 1. However, $|i\rangle$ is not an eigenstate of the Hamiltonian of the chain of spins with nearest-neighbour interactions

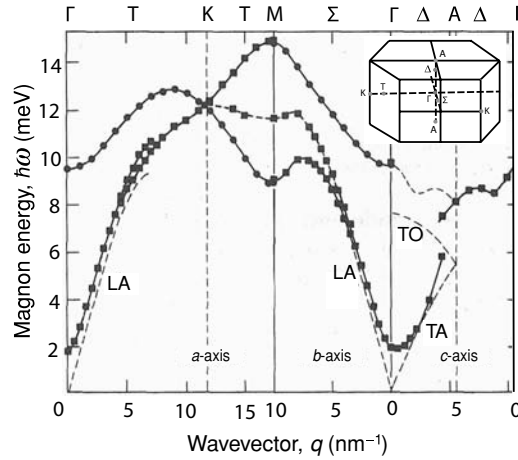
$$\mathcal{H} = -2\mathcal{J} \sum_{i=1}^{N-1} [S_i^z S_{i+1}^z + \frac{1}{2}(S_i^+ S_{i+1}^- + S_i^- S_{i+1}^+)]$$

because $\mathcal{H}|i\rangle = 2\mathcal{J}[-(N-1)S^2 + 2S|i\rangle - S|i+1\rangle - S|i-1\rangle]$. It is necessary to form linear combinations like

$$|q\rangle = \frac{1}{\sqrt{N}} \sum_i e^{iq \cdot \mathbf{r}_i} |i\rangle \quad (5.59)$$

Figure 5.26

Magnon dispersion relation for terbium (J. Jonsen and A. R. Mackintosh, *Rare Earth Magnetism*, Oxford University Press 1991).



This state is a magnon, a spin flip delocalized on the chain, with wavevector \mathbf{q} . Then

$$\begin{aligned} \mathcal{H}|\mathbf{q}\rangle &= \frac{2\mathcal{J}}{\sqrt{N}} \sum_{i=1}^{N-1} e^{i\mathbf{q}\cdot\mathbf{r}_i} [-(N-1)S^2 + 2S|i\rangle - S|i+1\rangle - S|i-1\rangle] \\ &= [-2\mathcal{J}(N-1)S^2 + 4\mathcal{J}S(1 - \cos qa)]|\mathbf{q}\rangle. \end{aligned} \quad (5.60)$$

Dropping the first term, which is constant, we have $\varepsilon(\mathbf{q}) = 4\mathcal{J}S(1 - \cos qa)$, as before.

Dispersion relations are best measured by inelastic neutron scattering, which is discussed in Chapter 10. There are multiple magnon branches when the unit cell is noncubic, or if it contains more than one magnetic atom. The energy in a mode of frequency $\omega_{\mathbf{q}}$ containing $N_{\mathbf{q}}$ magnons is $(N_{\mathbf{q}} + \frac{1}{2})\hbar\omega_{\mathbf{q}}$. Excitation of magnons is responsible for the fall of magnetization with increasing T . They also contribute to resistivity and magnetic specific heat. By analysing spin-wave dispersion relations measured across the Brillouin zone, it is possible to deduce the exchange interactions $\mathcal{J}(\mathbf{r}_{ij})$ for different atom pairs. Alternatively, the wavevector-dependent exchange $\mathcal{J}(\mathbf{q})$ can be fitted to the data. When the minimum of $\mathcal{J}(\mathbf{q})$ does not fall at $q = 0$, a spatially modulated magnetic structure is stable (§6.3).

Figure 5.26 shows the spin-wave dispersion relation for terbium. There is an energy gap at $q = 0$ due to the single-ion anisotropy of this rare-earth metal (§4.4.4). Excitation of spin waves can be suppressed at very low temperatures by the anisotropy. The energy gap at $q = 0$ is K_1/n , where n is the number of atoms per unit volume. In hexagonal close packed (hcp) cobalt, for example, $n = 9 \times 10^{28} \text{ m}^{-3}$, $K_1 = 500 \text{ kJ m}^{-3}$, the spin-wave gap is 0.4 K.

Magnons behave like bosons; each magnon corresponds to the reversal of one spin $\frac{1}{2}$ over the whole sample, or a change $\Delta M_S = 1$ for the whole system. Hence the average number of quantized spin waves in a mode \mathbf{q} is given by the

Table 5.6. Comparison of excitations in solids

Excitation		Dispersion	Specific heat
Electrons	Fermions	$\varepsilon_k \approx (\hbar/2m)k^2$	γT
Phonons	Bosons	$\varepsilon_q \approx c_0 q$	T^3
Magnons (ferromagnetic)	Bosons	$\varepsilon_q \approx D_{sw} q^2$	$T^{3/2}$
Magnons (antiferromagnetic)	Bosons	$\varepsilon_q \approx D_{af} q$	T^3

Bose distribution

$$\langle N_q \rangle = 1/[\exp(\hbar\omega_q/k_B T) - 1].$$

However, the magnon density of states $\mathcal{N}(\omega_q) \propto \omega_q^{\frac{1}{2}}$, just like that of electrons which have a similar dispersion relation $\varepsilon_k = \hbar^2 k^2 / 2m$. Dispersion relations and the corresponding low-temperature specific heats are summarized in Table 5.6. It can be shown that the reduction in magnetization at low temperatures due to the excitation of magnons is

$$\Delta M/M_0 = (0.0587/\nu)(k_B T/2S\mathcal{J})^{3/2}. \quad (5.61)$$

This is the Bloch $T^{3/2}$ power law. The integer ν equals 1, 2 or 4 for a simple cubic, bcc or fcc lattice. Specific heat follows the same power law at low temperature. A consequence of spin-wave excitation is that Curie temperatures are much lower than expected from molecular field theory, given the exchange constant \mathcal{J} (Fig. 5.23).

For electrons in ferromagnetic metals, there is an additional scattering process, in addition to scattering from defects, phonons and other electrons. The electron can be inelastically spin-flip scattered, with the creation or annihilation of a magnon (ω_q, \mathbf{q}). This leads to a term in resistivity varying as T^2 .

Our discussion of spin waves has been based on localized spins and Heisenberg exchange coupling, but the idea is more general; any ferromagnetic continuum with exchange stiffness will exhibit spin-wave excitations.

5.4.2 Stoner excitations

Besides spin waves, another type of excitation in a metal can reduce its magnetization. Electrons at the Fermi level can be excited from filled states in the majority-spin band to empty states in the minority-spin band. If the initial state has wavevector \mathbf{k} and the final state has wavevector $\mathbf{k} - \mathbf{q}$, an excitation of wavevector \mathbf{q} is produced. The energy of the excitation is given by

$$\hbar\omega_q = \varepsilon_k - \varepsilon_{k-q} + \Delta_{ex}.$$